Altered m^{6}A Modification of Specific Cellular Transcripts Affects *Flaviviridae* Infection

Nandan S. Gokhale,[1,9] Alexa B.R. McIntyre,[3,4,9] Melissa D. Mattocks,[5] Christopher L. Holley,[1,2] Helen M. Lazear,[5] Christopher E. Mason,[3,6,7,8,*] and Stacy M. Horner[1,2,10,*]

[1]Department of Molecular Genetics and Microbiology, Duke University Medical Center, Durham, NC 27705, USA
[2]Department of Medicine, Duke University Medical Center, Durham, NC 27705, USA
[3]Department of Physiology and Biophysics and the Institute for Computational Biomedicine, Weill Cornell Medicine, New York, NY 10065, USA
[4]Tri-Institutional Program in Computational Biology and Medicine, New York, NY 10065, USA
[5]Department of Microbiology and Immunology, University of North Carolina at Chapel Hill, Chapel Hill, NC 27599, USA
[6]The HRH Prince Alwaleed Bin Talal Abdulaziz Alsaud Institute for Computational Biomedicine, Weill Cornell Medicine, New York, NY 10065, USA
[7]The WorldQuant Initiative for Quantitative Prediction, Weill Cornell Medicine, New York, NY 10065, USA
[8]The Feil Family Brain and Mind Research Institute, Weill Cornell Medicine, New York, NY 10065, USA
[9]These authors contributed equally
[10]Lead Contact
*Correspondence: chm2042@med.cornell.edu (C.E.M.), stacy.horner@duke.edu (S.M.H.)
https://doi.org/10.1016/j.molcel.2019.11.007

SUMMARY

The RNA modification *N*^{6}-methyladenosine (m^{6}A) modulates mRNA fate and thus affects many biological processes. We analyzed m^{6}A across the transcriptome following infection by dengue virus (DENV), Zika virus (ZIKV), West Nile virus (WNV), and hepatitis C virus (HCV). We found that infection by these viruses in the *Flaviviridae* family alters m^{6}A modification of specific cellular transcripts, including *RIOK3* and *CIRBP*. During viral infection, the addition of m^{6}A to *RIOK3* promotes its translation, while loss of m^{6}A in *CIRBP* promotes alternative splicing. Importantly, viral activation of innate immune sensing or the endoplasmic reticulum (ER) stress response contributes to the changes in m^{6}A in *RIOK3* or *CIRBP*, respectively. Further, several transcripts with infection-altered m^{6}A profiles, including *RIOK3* and *CIRBP*, encode proteins that influence DENV, ZIKV, and HCV infection. Overall, this work reveals that cellular signaling pathways activated during viral infection lead to alterations in m^{6}A modification of host mRNAs to regulate infection.

INTRODUCTION

Transcriptional and post-transcriptional regulatory mechanisms influence gene expression in cells following infection by viruses, including those in the *Flaviviridae* family. The *Flaviviridae* family of positive-sense RNA viruses includes dengue virus (DENV), Zika virus (ZIKV), West Nile virus (WNV), and hepatitis C virus (HCV), all of which cause significant mortality and morbidity worldwide (Holbrook, 2017; Thrift et al., 2017). Previous studies have shown broad changes in cellular transcript levels during *Flaviviridae* infection that highlight a complex relationship between viral infection and gene expression, whereby the host attempts to resist infection by up- or downregulating relevant genes while viruses co-opt host transcription to facilitate replication and avoid host defenses (Fink et al., 2007; Kumar et al., 2016; Rosenberg et al., 2018; Sessions et al., 2013; Su et al., 2002; Zanini et al., 2018). Differential expression of proviral and antiviral host factors is therefore an important determinant of the outcome of *Flaviviridae* infection.

Host gene expression during *Flaviviridae* infection can be tuned by post-transcriptional RNA controls (De Maio et al., 2016; Luna et al., 2015; Schwerk et al., 2015). One of these controls is the chemical modification of RNA (Gilbert et al., 2016). The most prevalent internal modification of mRNA is *N*^{6}-methyladenosine (m^{6}A). The regulation of m^{6}A in RNA is controlled by specific cellular proteins. The METTL3-METTL14-WTAP "writer" complex catalyzes the methylation of adenosine residues in mRNA, targeting the consensus motif DRA*CH (where D = G/A/U, R = G/A, H = U/A/C, and * denotes modified A) in mRNA for methylation; however, how specific DRACH motifs are selected for modification is still not well understood (Meyer and Jaffrey, 2017; Shi et al., 2019; Yang et al., 2018). "Reader" RNA-binding proteins recognize m^{6}A to modulate mRNA metabolism, including mRNA splicing, nuclear export, stability, translation, and structure (Meyer and Jaffrey, 2017; Shi et al., 2019; Yang et al., 2018). By regulating specific transcripts, m^{6}A affects many important biological processes (Gonzales-van Horn and Sarnow, 2017; Meyer and Jaffrey, 2017; Shi et al., 2019; Yang et al., 2018).

Viral infection can be influenced by m^{6}A modification of either viral or host transcripts. Transcripts from both DNA and RNA viruses can be methylated, and m^{6}A in these RNAs has various proviral and antiviral functions (Courtney et al., 2017; Gokhale et al., 2016; Gokhale and Horner, 2017; Hao et al., 2019; Imam et al., 2018; Kennedy et al., 2016; Lichinchi et al., 2016a,

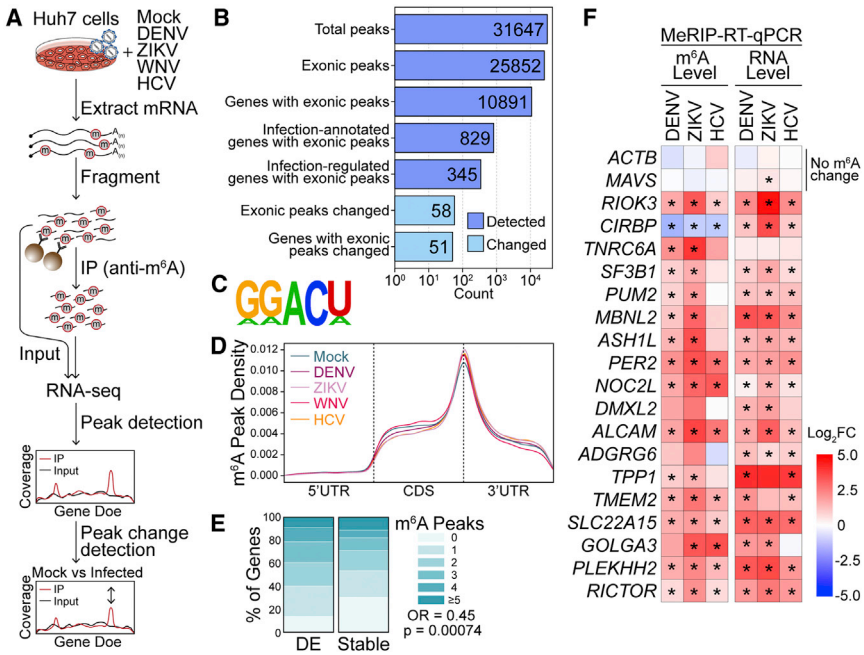

Figure 1. *Flaviviridae* Infection Alters m^{6}A Modification of Specific Transcripts

(A) Schematic of the MeRIP-seq protocol used to identify differential m^{6}A methylation following infection of Huh7 cells with DENV, ZIKV, WNV, and HCV. RNA was harvested at 48 h post-infection (hpi), and experiments were performed in triplicate.

(B) The number of peaks and genes with m^{6}A peaks detected in ≥ 2 mock- or virus-infected samples (dark blue; MACS2 q value < 0.05) and peaks that change during infection (light blue, |peak – gene Log_2FC| ≥ 1, adjusted p < 0.05). "Infection-annotated genes": genes with known annotations for the reactome pathways "infectious disease," "unfolded protein response," "interferon signaling," or "innate immune signaling" in the database used by fgsea. "Infection-regulated genes": genes that show a Log_2FC in gene expression ≥ 2 in RNA expression between mock- and virus-infected samples (adjusted p < 0.05).

(C) The most significantly enriched motif in the MeRIP fractions across all samples (HOMER, p = 1e-831).

(D) Metagene plot of "methylated" DRACH motifs (detected in a peak in at least two replicates) across transcripts in mock- and virus-infected cells.

(E) The percent of genes with m^{6}A peaks that changed expression with infection (|Log_2FC| ≥ 2, adjusted p < 0.05, N = 137) and genes that remained stable (|Log_2FC| < 0.5, adjusted p > 0.05, N = 7627) for transcripts with mean expression ≥ 50 reads.

(F) (Left) MeRIP-qRT-PCR analysis of relative m^{6}A level of transcripts with infection-altered m^{6}A modification or controls (*ACTB* and *MAVS*) in DENV, ZIKV, and HCV-infected (48 hpi) Huh7 cells. (Right) RNA expression of these transcripts relative to *GAPDH*. Values in heatmap are the mean of 3 independent experiments. *p < 0.05, by unpaired Student's t test.

See also Figure S1 and Tables S1 and S2.

2016b; McIntyre et al., 2018; Rubio et al., 2018; Tirumuru et al., 2016; Tsai et al., 2018; Williams et al., 2019; Winkler et al., 2019; Ye et al., 2017). m^{6}A in specific cellular transcripts is also important during viral infection (Liu et al., 2019b; Rubio et al., 2018; Winkler et al., 2019). For example, m^{6}A regulates the antiviral *IFNB1* transcript (Rubio et al., 2018; Winkler et al., 2019). However, the role of m^{6}A in cellular mRNA during viral infection is still not well understood, in part because of difficulties in accurately and quantitatively mapping the modification. While several viruses alter m^{6}A modification in cellular mRNAs (Hesser et al., 2018; Lichinchi et al., 2016a, 2016b; Tan et al., 2018), the scale of these changes has likely been overestimated (McIntyre et al., 2019). Moreover, there are almost no data on common m^{6}A changes in host mRNA across multiple viruses, and the functional consequences of m^{6}A changes in cellular mRNA during viral infection have also not been examined. Therefore, identifying both m^{6}A changes during viral infection and the consequences of these changes on cellular mRNA are important for understanding post-transcriptional regulation of the host response to infection.

Here, we studied the effect of DENV, ZIKV, WNV, and HCV infection on the m^{6}A epitranscriptome. We found that infection by all four viruses led to altered m^{6}A modification of a set of specific cellular transcripts and that activation of innate immunity and endoplasmic reticulum (ER) stress responses by infection contribute to differential m^{6}A modification and changes in translation or splicing of these transcripts. Importantly, transcripts with altered m^{6}A encode proteins that regulate infection, indicating that post-transcriptional gene regulation of mRNA by m^{6}A has the potential to affect host response and viral replication.

RESULTS

Flaviviridae Infection Alters m^{6}A Modification of Specific Cellular Transcripts

Flaviviridae infection changes the expression of proviral and antiviral gene products (Fink et al., 2007; Kumar et al., 2016; Rosenberg et al., 2018; Sessions et al., 2013; Su et al., 2002; Zanini et al., 2018). Since m^{6}A can modulate RNA fate, and therefore protein expression, we hypothesized that altered m^{6}A modification would influence expression of host genes that regulate viral infection. We therefore measured changes in the m^{6}A modification of host transcripts during *Flaviviridae* infection using methylated RNA immunoprecipitation and sequencing (MeRIP-seq) (Figure 1A). For MeRIP-seq, we used an anti-m^{6}A antibody to enrich m^{6}A-modified RNA fragments prior to RNA sequencing of both the input and immunoprecipitated (IP) fractions (Dominissini et al., 2012; Meyer et al., 2012). We note that this antibody also recognizes the similar modification N^6,2′-*O*-dimethyladenosine (m^{6}A$_m$), which in mRNA is only found in the 5′ cap (Linder et al., 2015; Mauer and Jaffrey, 2018). We performed MeRIP-seq on RNA from human Huh7 liver hepatoma cells, which are permissive for all four viruses, at 48 h post-infection. At this time point, 60%–90% of cells stained positive for viral antigen (Figure S1A). We first identified gene expression changes in

response to infection. We analyzed differential expression of genes between infected samples and uninfected controls using the input fractions from MeRIP-seq and found 50 genes that were differentially expressed (DESeq2, adjusted $p < 0.05$, $|Log_2\text{-Fold Change (FC)}| \geq 2$) across all four viruses (Figures S1B and S1C; Table S1). We found that several pathways were similarly altered by all four viruses (Figure S1D), including innate immunity (such as NF-κB, TNF, and MAPK signaling) and the ER stress response. These results, which we validated by qRT-PCR (Figure S1E), are similar to what has been reported for individual *Flaviviridae* (Carletti et al., 2019; Fink et al., 2007; Kumar et al., 2016; Rosenberg et al., 2018; Sessions et al., 2013; Su et al., 2002; Zanini et al., 2018).

We then predicted m^{6}A-modified regions within mRNAs by calling peaks in IP over input RNA-seq coverage across transcripts using MACS2, a ChIP-seq peak caller commonly used to detect m^{6}A peaks from MeRIP-seq data (McIntyre et al., 2019; Zhang et al., 2008). We detected a total of 31,647 peaks, with 25,852 exonic peaks corresponding to 10,891 genes across all uninfected and infected samples (Figure 1B). The known m^{6}A motif DRACH (in particular, GGACU) was enriched under the identified peaks (Figure 1C). As expected, detected peaks were most common at the end of the coding sequence and beginning of the 3′ untranslated region (UTR) (Figure 1D) (Meyer and Jaffrey, 2017). We did not observe a change in the distribution of m^{6}A across transcript regions with DENV, ZIKV, WNV, or HCV infection (Figure 1D). This is in contrast to a previous report that suggested ZIKV infection led to increased methylation in the 5′ UTRs of cellular transcripts (Lichinchi et al., 2016b); however, we also did not detect a difference in m^{6}A distribution in 5′ UTRs following ZIKV infection on reanalysis of that published data using two different peak callers: MACS2 or MeTDiff (Figure S1F) (Cui et al., 2018). Further, following viral infection, we found only subtle changes in the overall level of m^{6}A relative to unmodified adenosine in purified mRNA, as analyzed by liquid chromatography-tandem mass spectrometry (LC-MS/MS) of digested nucleotides, and no change in the expression of cellular m^{6}A machinery, as analyzed by immunoblotting (Figures S1G and S1H). Indeed, since the expression of the methylation machinery was not changed by infection, we would not predict broad, unidirectional changes in the abundance or distribution of m^{6}A in cellular mRNAs.

However, functional annotation of the m^{6}A-modified genes expressed in the infected samples did reveal an enrichment for genes with roles in infection. In total, 829 methylated genes were annotated as involved in the reactome pathways of "infectious disease," "unfolded protein response," "interferon signaling," or "innate immune system" ("infection-annotated genes"; see STAR Methods; Figure 1B). Further, 345 methylated genes were differentially expressed between infected and uninfected samples ("infection-regulated genes"; Figure 1B). Indeed, mRNAs that changed expression with infection ($p\ adj < 0.05$, $|Log_2FC| \geq 2$, mean expression ≥ 50) were more likely to have at least one m^{6}A site than those that did not change expression ($p\ adj > 0.05$, $|Log_2FC| < 0.5$, mean expression ≥ 50; Fisher's exact test $p = 0.00074$, odds ratio = 0.64) (Figure 1E). These results support previous reports that transcripts that undergo dynamic regulation tend to contain more m^{6}A sites than stable housekeeping mRNAs (Schwartz et al., 2014) and suggest that m^{6}A may regulate genes implicated in infection.

We next determined changes in m^{6}A from differences in IP enrichment relative to gene expression with infection by all four viruses. We detected shared m^{6}A changes in 58 exonic peaks in 51 genes following infection, most of which showed increases in m^{6}A and occurred in the 3′ UTR or coding sequence (Figure 1B; Table S2). While differentially expressed genes were enriched for pathways with known roles in infection (Figure S1D), genes that showed changes in methylation did not show enrichment for functional categories relevant to infection. We and others previously showed that MeRIP-qRT-PCR with primers under the changed m^{6}A peaks can detect relative changes in m^{6}A (Engel et al., 2018; McIntyre et al., 2019). Therefore, we used this method to orthogonally validate 18 of the predicted m^{6}A changes following infection. In these and subsequent analyses, we focused on m^{6}A changes following DENV, ZIKV, and HCV infection. Of these 18 transcripts, 16 showed a significant change in m^{6}A relative to any change in gene expression with at least two viruses, and 9 of those showed a significant change with all three viruses. Most non-significant m^{6}A changes trended toward the change predicted by MeRIP-seq (Figure 1F). *ACTB* and *MAVS* mRNAs, both predicted to be stably methylated during infection, indeed showed no m^{6}A changes (Figure 1F).

For our predictions of pan-viral m^{6}A changes using MeRIP-seq (above), we compared all infected to all uninfected replicates for increased statistical power (McIntyre et al., 2019). However, to also detect any peak changes unique to single viruses, we used the same computational approach described above (Table S2). MeRIP-qRT-PCR for these putative virus-specific peaks (two per virus) showed similar changes in relative m^{6}A at those peaks with infection by all three viruses tested, rather than individual virus-mediated changes, in the same direction as predicted by MeRIP-seq (Figure S1I). This suggests that m^{6}A regulation can occur through common processes activated by viral infection. Together, our data reveal that hundreds of transcripts differentially expressed during *Flaviviridae* infection contain m^{6}A and that infection alters m^{6}A modification of specific host transcripts.

Flaviviridae Infection Alters m^{6}A Modification of *RIOK3* and *CIRBP* mRNA through Distinct Pathways

We focused on two specific transcripts that gain and lose m^{6}A (*RIOK3* and *CIRBP*, respectively) during infection by all viruses for further analysis. *RIOK3* encodes a serine/threonine kinase that may regulate antiviral signaling (Feng et al., 2014; Takashima et al., 2015; Willemsen et al., 2017), while *CIRBP* encodes a stress-induced RNA-binding protein (Liao et al., 2017). Following viral infection, *RIOK3* mRNA gains an m^{6}A peak in the 3′ UTR near the stop codon (Figure 2A), and *CIRBP* mRNA loses an m^{6}A peak in the coding sequence of its last exon (Figure 2B). The *RIOK3* and *CIRBP* peaks span four and three DRACH motifs, respectively. Both peaks appear in published datasets: the *RIOK3* peak in mouse liver tissue (Zhou et al., 2018) and the *CIRBP* peak in HepG2 cells (Huang et al., 2019; Zhong et al., 2018). We performed MeRIP-qRT-PCR on RNA from cells infected with DENV, ZIKV, and HCV to validate these m^{6}A changes. MeRIP-qRT-PCR confirmed that the relative m^{6}A

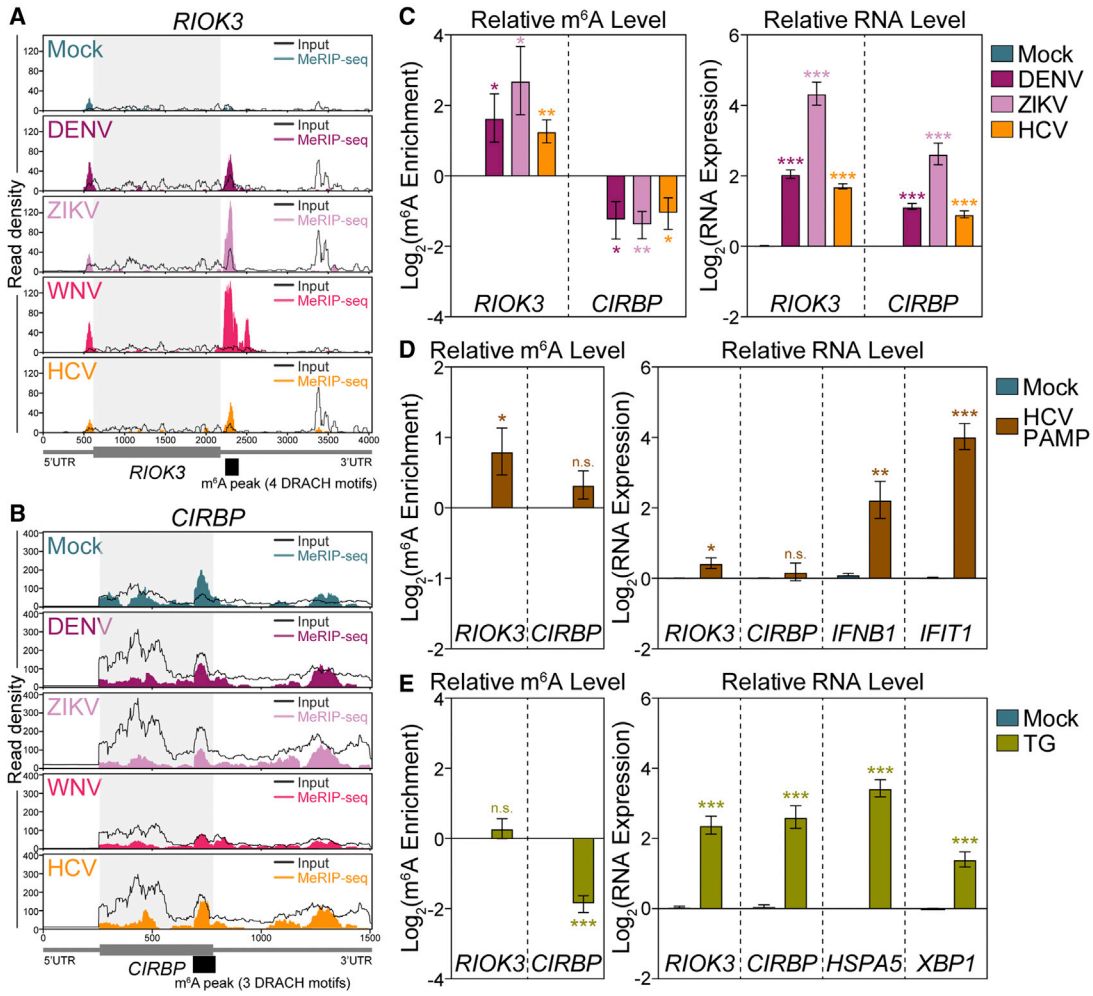

Figure 2. *Flaviviridae* Infection Alters m^{6}A Modification of *RIOK3* and *CIRBP* mRNA through Distinct Cellular Pathways

(A and B) Coverage plot of MeRIP (color) and input (black) reads in (A) *RIOK3* and (B) *CIRBP* transcripts in Huh7 cells infected with the indicated virus (48 hpi), as determined by MeRIP-seq. Representative of three biological replicates. Infection-altered m^{6}A peaks are indicated in black under the transcript map.

(C) (Left) MeRIP-qRT-PCR analysis of relative m^{6}A level of *RIOK3* and *CIRBP* in mock- and virus-infected (48 hpi) Huh7 cells. (Right) RNA expression of *RIOK3* and *CIRBP* relative to *HPRT1*.

(D) (Left) MeRIP-qRT-PCR analysis of relative m^{6}A level of *RIOK3* and *CIRBP* in mock- and HCV PAMP-transfected (8 h) Huh7 cells. (Right) RNA expression of *RIOK3*, *CIRBP*, as well as positive control transcripts *IFNB1* and *IFIT1* relative to *HPRT1*.

(E) (Left) MeRIP-qRT-PCR analysis of relative m^{6}A level of *RIOK3* and *CIRBP* in mock- and thapsigargin-treated (TG; 16 h) Huh7 cells. (Right) RNA expression of *RIOK3*, *CIRBP*, and positive control transcripts *HSPA5* and *XBP1* relative to *HPRT1*. Values are the mean ± SEM of 6 (C and D), or 5 (E) biological replicates. *p < 0.05, **p < 0.01, ***p < 0.001 by unpaired Student's t test. ns, not significant.

See also Figure S2 and Tables S2 and S3.

modification of *RIOK3* was significantly increased and that of *CIRBP* decreased after infection, while *RIOK3* and *CIRBP* mRNA levels both increased (Figures 1F and 2C). These m^{6}A changes in *RIOK3* and *CIRBP* were also apparent in chromatin-associated RNA following ZIKV infection, suggesting that the regulation of m^{6}A at these sites occurs co-transcriptionally (Ke et al., 2017; Slobodin et al., 2017) (Figure S2A). In uninfected cells, both *RIOK3* and *CIRBP* transcripts are bound by the m^{6}A-binding protein YTHDF1 (Figures S2B and S2C). However, DENV, ZIKV, and HCV infection increased YTHDF1 association with *RIOK3* and decreased its association with *CIRBP*, suggesting that YTHDF1 recognizes the altered m^{6}A status of *RIOK3* and *CIRBP* transcripts following infection (Figure S2D).

We next investigated whether cellular pathways stimulated by viral infection (Figure S1D) contribute to the virally induced m^{6}A changes in *RIOK3* and *CIRBP*. *Flaviviridae* infection drives signaling cascades that lead to the induction of interferon-β (IFN) and antiviral IFN-stimulated genes (ISGs) by IRF3 (Horner and Gale, 2013; Muñoz-Jordán and Fredericksen, 2010; Suthar et al., 2013). In infected Huh7 IRF3 KO cells (Vazquez et al., 2019), the increase in *RIOK3* m^{6}A with infection was attenuated (from ~4- to ~1.5-fold) compared to parental cells (Figures S2E and 2C). However, DENV and ZIKV infection of IRF3 KO cells still

reduced the relative m^{6}A enrichment of *CIRBP*, consistent with that seen following infection of the parental cells (Figures S2E and 2C) (Vazquez et al., 2019). This suggests that IRF3 activation contributes to increased *RIOK3* m^{6}A modification while not affecting the m^{6}A status of *CIRBP*. To determine if innate immune activation in the absence of replicating virus alters m^{6}A modification of *RIOK3* and *CIRBP*, we measured the relative m^{6}A levels of *RIOK3* and *CIRBP* mRNA by MeRIP-qRT-PCR following transfection of Huh7 cells with an HCV immunostimulatory RNA (HCV PAMP) (Saito et al., 2008). HCV PAMP induced expression of *IFNB1* and the ISG *IFIT1* and also increased m^{6}A modification of *RIOK3* but did not decrease *CIRBP* methylation (Figure 2D). Importantly, we found that the increase in *RIOK3* m^{6}A following HCV PAMP was dependent on the m^{6}A methyltransferases METTL3 and METTL14, as HCV PAMP did not increase m^{6}A modification of *RIOK3* following depletion of *METTL3* and *METTL14* (Figure S2F). IFN-β treatment, which activates the IFN response, also led to a slight but significant increase in the relative m^{6}A enrichment of *RIOK3* but not *CIRBP* (Figure S2G). These data indicate that signaling through innate immune sensing and response pathways promotes the m^{6}A modification of *RIOK3* mRNA following infection.

We next sought to define the signaling pathways that lead to reduced m^{6}A modification of *CIRBP* mRNA. We and others have shown that *Flaviviridae* infection activates the ER stress response (Figure S1D) (Blázquez et al., 2014; Carletti et al., 2019; Chan, 2014; Neufeldt et al., 2018). To test whether ER stress alters the m^{6}A modification of *CIRBP* or *RIOK3*, we measured their relative m^{6}A levels following treatment of cells with thapsigargin (TG; Figure 2E), an ER Ca^{2+} ATPase inhibitor that induces an ER stress response (Lee et al., 2012). TG increased the mRNA level of both *RIOK3* and *CIRBP* and that of the positive controls *HSPA5* and *XBP1* by about 4-fold (Figure 2E). Further, TG reduced m^{6}A modification of *CIRBP*, similar to what we observed with viral infection, while not changing the relative m^{6}A level of *RIOK3* (Figure 2E). Together, these data reveal that innate immune and ER stress signaling, both of which are activated during *Flaviviridae* infection, can divergently influence the m^{6}A methylation program and can separately affect m^{6}A modification of specific transcripts.

To define the mRNAs that have altered m^{6}A in response to innate immune or ER stress signaling, we also performed MeRIP-seq analysis on mRNA from Huh7 cells treated with HCV PAMP or TG. Both of these treatments led to m^{6}A peak changes in a subset of mRNAs (Figure S2H; Table S3). The m^{6}A peaks detected in these data did not necessarily correspond to peaks called in the infection data (Table S2), likely because the reproducibility of individual MeRIP-seq peaks is low (McIntyre et al., 2019). Therefore, we calculated differences in m^{6}A enrichment with HCV PAMP and TG at the 31,467 regions previously identified as m^{6}A peaks in the infection data ($|\text{Log}_2\text{FC} > 1|$ and threshold of $p < 0.1$). We observed five infection-altered peaks that were also changed by TG, including the *CIRBP* peak, and three infection-altered peaks also changed with HCV PAMP (Figure S2I). All of these changes were in the same direction as observed with infection. The infection-induced m^{6}A peak in *RIOK3* did show an increase in m^{6}A enrichment at the same region with HCV PAMP, but it was not statistically significant, perhaps because the m^{6}A changes observed with HCV PAMP were smaller than those observed with infection (Figures 2C and 2D). These results reveal that innate immune and ER stress signaling drive a portion of the m^{6}A changes we observed during *Flaviviridae* infection.

m^{6}A Modification Enhances RIOK3 Protein Expression during Infection

We next investigated the function of m^{6}A in *RIOK3* mRNA during infection. Consistent with our finding that DENV, ZIKV, and HCV infection all increased *RIOK3* mRNA levels (Figure 2C), RIOK3 protein expression also increased following infection (Figure 3A). m^{6}A can alter mRNA nuclear export, stability, and translation, all of which could regulate protein expression (Meyer and Jaffrey, 2017; Yang et al., 2018). We found no significant change in the nuclear export or mRNA stability of *RIOK3* during infection (Figures S3A and S3B). However, we did detect increased nascent translation of RIOK3 in DENV-infected cells compared to uninfected cells as measured by ^{35}S labeling of nascent proteins followed by RIOK3 protein immunoprecipitation, suggesting that RIOK3 translation was increased by infection (Figure 3B). This is consistent with our finding that during infection *RIOK3* mRNA has increased binding to the m^{6}A reader protein YTHDF1, which can promote translation of bound mRNAs under specific conditions (Figure S2D) (Han et al., 2019; Shi et al., 2018; Wang et al., 2015, 2019). To directly test whether YTHDF1 promotes *RIOK3* translation, we measured RIOK3 protein levels following DENV infection in cells depleted of YTHDF1. We found that YTHDF1 depletion prevented the DENV-induced increase in RIOK3 protein expression (Figure 3C). *RIOK3* translation increased during *Flaviviridae* infection, even though these viruses generally inhibit global cellular translation and induce the phosphorylation of the eukaryotic translation initiation factor eIF2α (Figure S3C) (Arnaud et al., 2010; Garaigorta and Chisari, 2009; Roth et al., 2017; Stern-Ginossar et al., 2019; Wek, 2018). Therefore, our results suggest that m^{6}A modification of *RIOK3* could allow this transcript to be efficiently translated during infection in a YTHDF1-dependent manner, despite global inhibition of translation.

To directly test whether m^{6}A can promote RIOK3 protein expression during infection, we generated Huh7 cell lines stably expressing a luciferase reporter that contains the wild-type (WT) *RIOK3* 3′ UTR, or an analogous 3′ UTR sequence in which all putative m^{6}A sites were abrogated by A→T mutations (m^{6}A-mut), downstream of a *Renilla* luciferase gene in which all DRACH motifs were ablated (m^{6}A null) (Figure 3D). These constructs also expressed a m^{6}A null Firefly luciferase gene whose expression is not regulated by m^{6}A. The WT *RIOK3* reporter had increased m^{6}A modification compared to the m^{6}A-mut *RIOK3* reporter following viral infection, as measured by MeRIP-qRT-PCR using primers that specifically amplified reporter RNA (Figure 3E). Therefore, the *RIOK3* 3′ UTR sequence is sufficient for m^{6}A addition following infection. Importantly, the relative luciferase activity of the WT *RIOK3* reporter was significantly increased compared to the m^{6}A-mut reporter following viral infection (Figure 3F). Taken together, these data reveal that m^{6}A modification of the 3′ UTR of *RIOK3* during infection promotes its translation during infection.

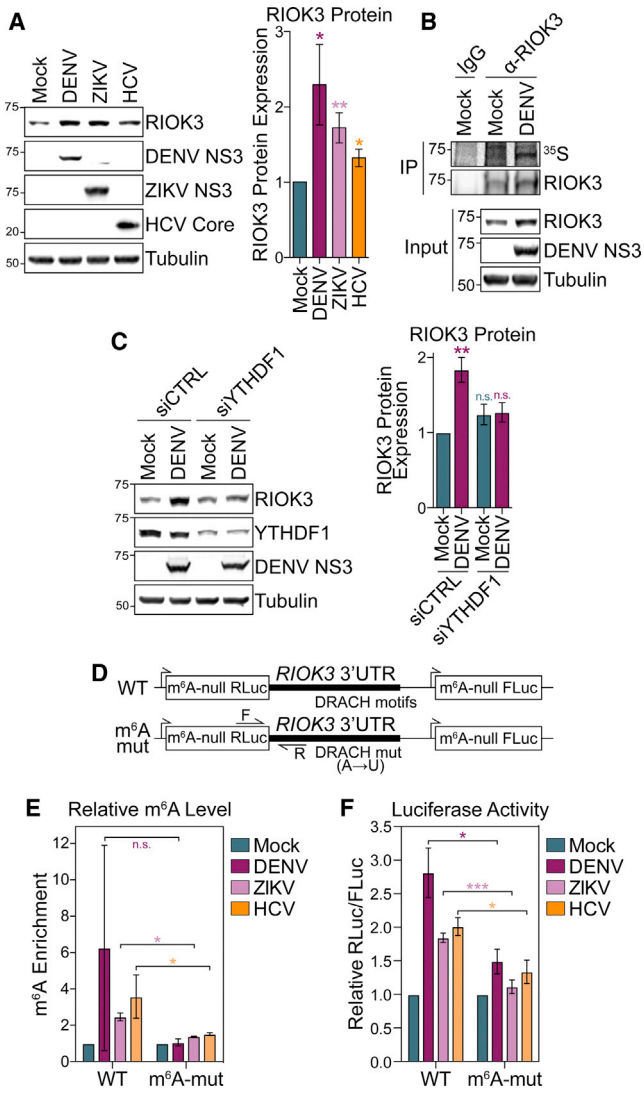

Figure 3. m^{6}A Promotes RIOK3 Protein Expression

(A) (Left) Representative immunoblot of RIOK3 protein expression in mock- and virus-infected (48 hpi) Huh7 cells. (Right) Quantification of RIOK3 protein expression relative to tubulin.

(B) Immunoprecipitation (IP) of RIOK3 from mock- and DENV-infected (48 hpi) Huh7 cells labeled with ^{35}S for 3 h. IP fractions were analyzed by autoradiography (^{35}S) and immunoblotting. Representative of 3 biological replicates.

(C) (Left) Representative immunoblot of RIOK3 protein expression in mock- and DENV-infected (48 hpi) Huh7 cells treated with non-targeting control (CTRL) or YTHDF1 siRNA. (Right) Quantification of RIOK3 protein expression relative to tubulin.

(D) Schematic of WT and mutant m^{6}A null *Renilla* luciferase (RLuc) *RIOK3* 3′ UTR reporters that also express m^{6}A null Firefly luciferase (FLuc) from a separate promoter. qRT-PCR primers (F and R) are indicated with arrows.

(E) MeRIP-qRT-PCR analysis of relative m^{6}A level of stably expressed WT and m^{6}A-mut *RIOK3* 3′ UTR reporter RNA in mock- and virus-infected (48 hpi) Huh7 cells.

(F) Relative luciferase activity (RLuc/FLuc) in mock- and virus-infected (48 hpi) Huh7 cells stably expressing WT and m^{6}A-mut *RIOK3* 3′ UTR reporters. Relative luciferase activity in uninfected cells was set as 1 for each reporter. Values are the mean ± SEM of 6 (A), 4 (C), 2 (E), or 5 (F) biological replicates. *$p < 0.05$, **$p < 0.01$, ***$p < 0.001$ by unpaired Student's t test. ns, not significant. See also Figure S3.

m^{6}A Modification Promotes Alternative Splicing of *CIRBP* mRNA during Infection

We then analyzed the function of reduced m^{6}A modification in *CIRBP* mRNA following infection. Neither the nuclear export nor the stability of *CIRBP* mRNA were affected following infection, suggesting that the loss of m^{6}A in *CIRBP* does not regulate these processes (Figures S4A and S4B). Based on our RNA-seq data, *CIRBP* encodes at least 2 isoforms: (1) the dominant, short isoform (*CIRBP-S*), which encodes a 172 aa, 18 kDa protein and (2) a long isoform in which an intron immediately downstream of the infection-altered m^{6}A peak and upstream of the stop codon is retained (*CIRBP-L*), resulting in a 297 aa, 32 kDa protein (Figure 4A; retained intron referred to as alternatively spliced region [ASR]). Interestingly, analysis of our RNA-seq data using MAJIQ (Vaquero-Garcia et al., 2016) to identify local splice variants suggested decreased retention of this intron during infection, which we confirmed in infected cells using qRT-PCR (Figure 4B). We observed a similar reduction of intron retention following TG treatment, which we had found also reduces *CIRBP* m^{6}A modification (Figures 4C and 2F). Indeed, both viral infection and TG treatment significantly reduced the protein level of CIRBP-L containing the retained intron, without affecting expression of CIRBP-S (Figures 4D and 4E). To test whether reduction of m^{6}A modification at the m^{6}A peak in *CIRBP* might affect alternative splicing of this transcript, we generated a splicing reporter wherein the m^{6}A null *Renilla* luciferase gene was fused to the WT genomic sequence of *CIRBP* from exon 5 onward (WT *CIRBP*) and a corresponding reporter in which the putative m^{6}A sites in the identified *CIRBP* m^{6}A peak were synonymously mutated (m^{6}A-mut *CIRBP*) (Figure 4F). Using qRT-PCR, we found that the m^{6}A-mut reporter had reduced intron retention compared to the WT reporter, revealing that the loss of m^{6}A in *CIRBP* regulates its alternative splicing and reduces the expression of the long isoform (Figure 4G).

To understand the purpose of alternative isoform usage of *CIRBP* during infection, we measured the polysome occupancy of the two *CIRBP* isoforms in response to infection. As expected, due to the global translation suppression known to occur during DENV (Roth et al., 2017), the size of the 80S peak was increased and polysomal peaks were decreased in DENV-infected cells (Figure S4C). *CIRBP-L* was not found in heavy polysome fractions in either uninfected or DENV-infected cells, suggesting that this transcript is inefficiently translated (Figure S4D). In contrast, *CIRBP-S* was found in heavy polysome fractions, but this association was reduced during DENV infection (Figure S4D). This suggests that *CIRBP-S* has reduced translation during infection. Given that the protein expression of CIRBP-S is not significantly reduced during infection (Figure 4D), reducing the expression of the inefficiently translated *CIRBP-L* isoform may represent a mechanism to ensure consistent production of CIRBP protein during viral infection.

m^{6}A-Altered Genes Regulate *Flaviviridae* Infection

Having found that both *RIOK3* and *CIRBP* transcripts have altered m^{6}A modification during infection, we tested whether their encoded protein products affect *Flaviviridae* infection. We depleted RIOK3 and CIRBP in Huh7 cells, infected these cells with DENV, ZIKV, or HCV, and then measured viral titer in the

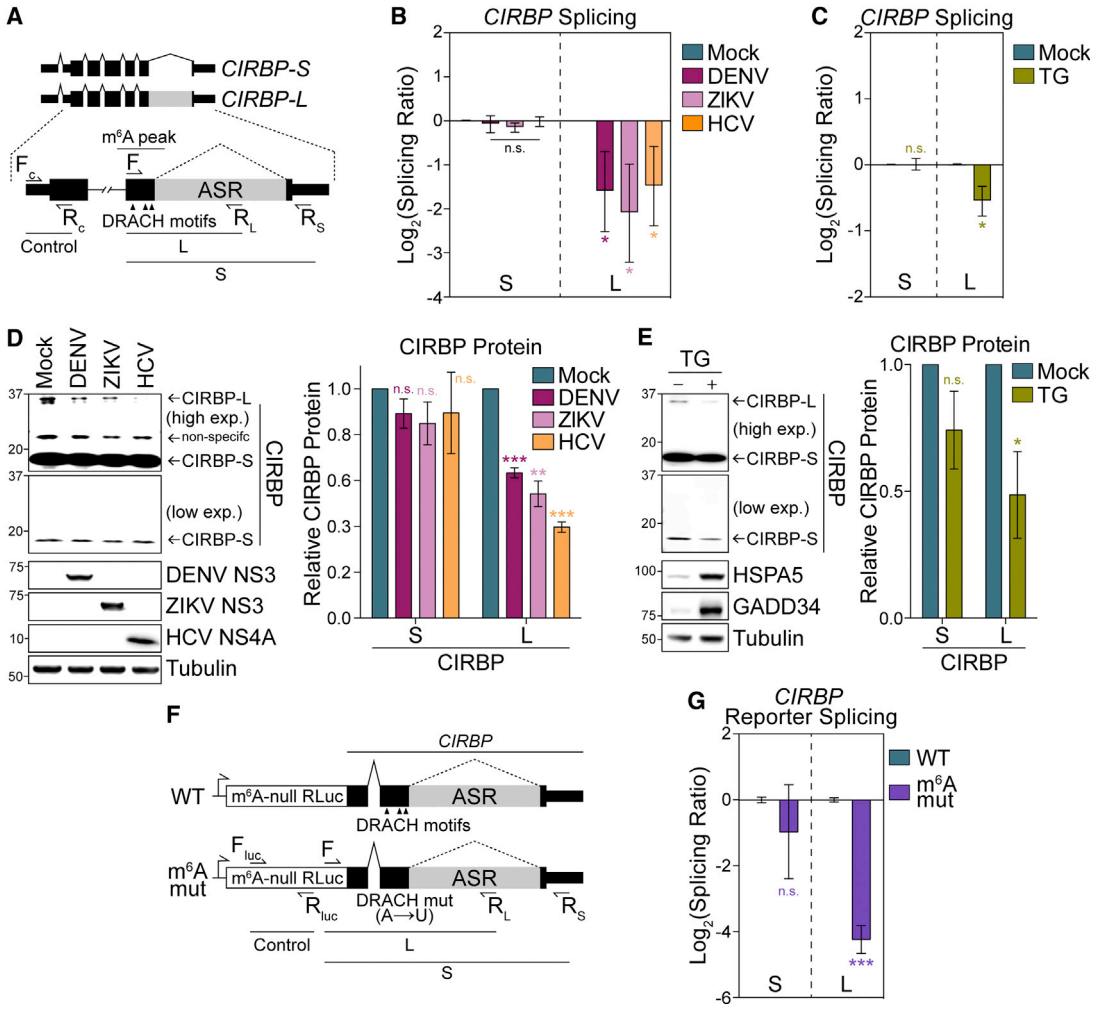

Figure 4. m^{6}A Promotes Alternative Splicing of *CIRBP*

(A) Schematic of *CIRBP* transcript isoforms with a focus on the alternatively spliced region (ASR). qRT-PCR primer locations are indicated with arrows (F_C-R_C: control *CIRBP* amplicon; F-R_L: long isoform specific; F-R_S: short isoform specific.

(B) qRT-PCR analysis of short (S) and long (L) *CIRBP* RNA isoforms in mock- and virus-infected (48 hpi) Huh7 cells relative to control *CIRBP* amplicon.

(C) qRT-PCR analysis of S and L *CIRBP* RNA isoforms in mock- and TG-treated (16 h) Huh7 cells.

(D) (Left) Representative immunoblot of short (CIRBP-S) and long (CIRBP-L) CIRBP protein isoforms in mock- and virus-infected (48 hpi) Huh7 cells. (Right) Quantification of CIRBP protein isoform expression relative to tubulin.

(E) (Left) Representative immunoblot analysis of CIRBP protein isoforms in mock- and TG-treated (500 nM, 16 h) Huh7 cells. HSPA5 and GADD34 are positive controls. (Right) Quantification of CIRBP protein isoform expression relative to tubulin.

(F) Schematic of WT and m^{6}A-mut *CIRBP* splicing reporters. qRT-PCR primer locations (F_{luc}-R_{luc}: control; F-R_L: long isoform specific; F-R_s: short isoform specific) are indicated with arrows.

(G) qRT-PCR analysis of *CIRBP* splicing reporter isoform expression (S and L) relative to control *RLuc* amplicon in Huh7 cells transfected with WT and m^{6}A-mut constructs. Values are the mean ± SEM of 3 (B, D, E, G) or 5 (C) biological replicates. *p < 0.05, **p < 0.01, ***p < 0.001 by unpaired Student's t test. ns, not significant.

See also Figure S4.

supernatant. siRNA treatment reduced both *RIOK3* and *CIRBP* mRNA levels by ~70% and did not affect cell viability (Figures S5A and S5B). We found that RIOK3 depletion significantly reduced the production of infectious DENV and ZIKV particles but increased the production of infectious HCV particles (Figure 5A). Consistent with these data, RIOK3 stably overexpressed in two different clonal cell lines had the opposite effect on DENV, ZIKV, and HCV infectious particle production (Figures 5B and 5C). This suggests that RIOK3 promotes DENV and ZIKV infection but inhibits HCV infection. However, the depletion of both the large and small isoforms of CIRBP, as well as only the large isoform of CIRBP, reduced the production of infectious DENV, ZIKV, and HCV (Figures 5D, S5C, and S5D), while overexpression of both the short and long isoforms of CIRBP in two different clonal cell lines each increased infection by these viruses (Figures 5E and 5F). This suggests that both CIRBP isoforms are

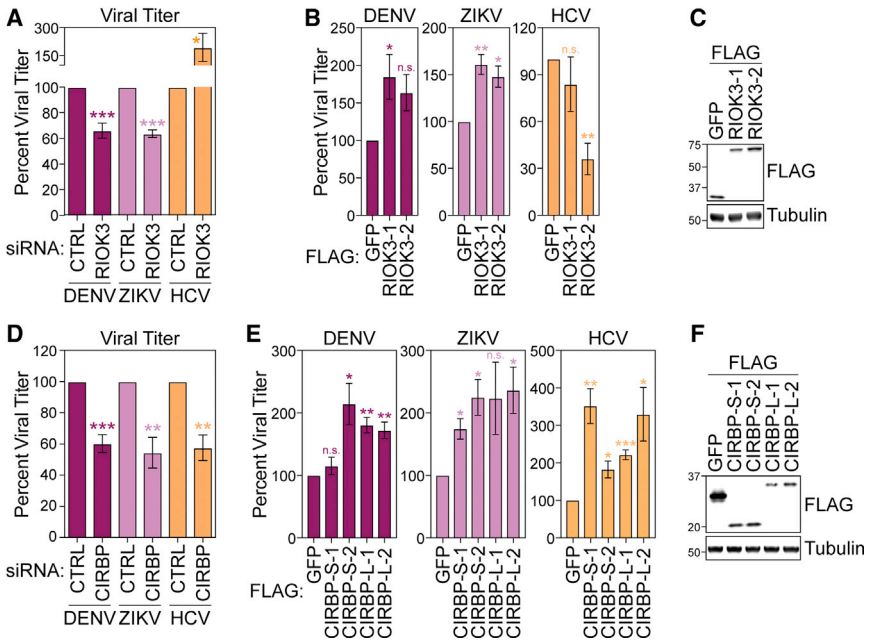

Figure 5. RIOK3 and CIRBP Regulate *Flaviviridae* Infection

(A) Focus-forming assay (FFA) of supernatants from DENV, ZIKV, or HCV-infected (72 hpi) Huh7 cells treated with non-targeting control (CTRL) or *RIOK3* siRNA.

(B) FFA of supernatants from DENV, ZIKV, or HCV-infected (72 hpi) Huh7 cells stably overexpressing FLAG-GFP or FLAG-RIOK3 (2 independent clones).

(C) Immunoblot analysis of cell lines in (B).

(D) FFA of supernatants harvested from DENV, ZIKV, or HCV-infected (72 hpi) Huh7 treated with CTRL or *CIRBP* siRNA.

(E) FFA of supernatants from DENV, ZIKV, or HCV-infected (72 hpi) Huh7 cells stably overexpressing FLAG-GFP or the short (FLAG-CIRBP-S) or long (FLAG-CIRBP-L) isoforms of CIRBP (2 independent clones).

(F) Immunoblot analysis of cell lines in (C). Values are the mean ± SEM of 4 (A and D) or 3 (B, E, and G) biological replicates. Viral infections were performed at a multiplicity of infection of 0.2. *$p < 0.05$, **$p < 0.01$, ***$p < 0.001$ by unpaired Student's t test. ns, not significant.

See also Figure S5.

proviral during DENV, ZIKV, and HCV infection. Interestingly, the CIRBP-S protein resides primarily in the nucleus, while CIRBP-L is predominantly cytoplasmic, irrespective of viral infection, which implicates distinct spatial regulation of proviral activity by CIRBP isoforms (Figure S5E).

We then performed a targeted siRNA screen to test whether other transcripts with infection-altered m^{6}A modification affect *Flaviviridae* infection. We depleted transcripts in which we had identified m^{6}A changes during infection (Figures 1F and S1I); infected these cells with DENV, ZIKV, or HCV; and measured cell viability, relative to RNA depletion levels, and the production of infectious virions in the supernatant (Figures 6 and S6A–S6C). We focused only on those transcripts that were depleted by at least 40% in our further analysis (21 out of 24 tested). For these, we found that 18/21 (86%) regulate at least one virus, while 10/21 (48%) affect at least two and 6/21 (29%) regulate all three viruses. For each virus, ~50% of m^{6}A-altered transcripts that we tested significantly increased or decreased infection. This indicates that m^{6}A can, as a general principle, tune the outcome of infection by modifying specific transcripts that regulate infection.

DISCUSSION

Here, we identify changes in m^{6}A methylation of cellular mRNAs during infection by viruses in the *Flaviviridae* family. We observed that infection by DENV, ZIKV, WNV, and HCV leads to changes in m^{6}A of a specific set of cellular transcripts, including some that encode factors that modulate *Flaviviridae* infection. We found that virus-induced pathways, including innate immune signaling and ER stress signaling, contribute to altered m^{6}A of several of these transcripts. Taken together, this work suggests that m^{6}A changes induced through cellular signaling pathways influence *Flaviviridae* infection.

We identified hundreds of m^{6}A-modified transcripts that were differentially expressed during infection or that were annotated as part of cellular pathways relevant for infection. These findings suggest that m^{6}A has the potential to post-transcriptionally regulate many genes during infection. Here, we focused on specific transcripts with virus-induced m^{6}A changes; we identified 58 peak changes in 51 transcripts following infection by DENV, ZIKV, WNV, and HCV. As our m^{6}A change analysis pipeline controls for changes in gene expression (McIntyre et al., 2019), these data should represent true changes in m^{6}A modification rather than changes in the expression of m^{6}A-modified transcripts. While changes in both m^{6}A modification and the expression of m^{6}A-modified transcripts are biologically relevant, identifying bona fide m^{6}A alterations during viral infection will allow us to understand how m^{6}A modification of cellular mRNA is regulated.

We found that the changes in m^{6}A methylation of *RIOK3*, *CIRBP*, and several other transcripts are driven by innate immune induction and the cellular response to ER stress, respectively. This suggests that these signals and likely other infection-induced pathways can be integrated into differential m^{6}A methylation activity and ultimately affect m^{6}A modification of cellular mRNAs. While expression changes in m^{6}A machinery affect m^{6}A modification during cancer and infection (Barbieri et al., 2017; Li et al., 2017b; Lin et al., 2016; Rubio et al., 2018; Vu et al., 2017; Winkler et al., 2019), this machinery did not change expression with *Flaviviridae* infection, pointing to a different mechanism for altered m^{6}A modification. Going forward, identifying the molecular mechanisms through which these signaling pathways lead to differential m^{6}A will be an important advance in understanding how the m^{6}A machinery acts on specific sites.

Our data suggest that virus-induced m^{6}A changes occur in nascent mRNA, which supports the hypothesis that m^{6}A is added co-transcriptionally and does not dynamically change

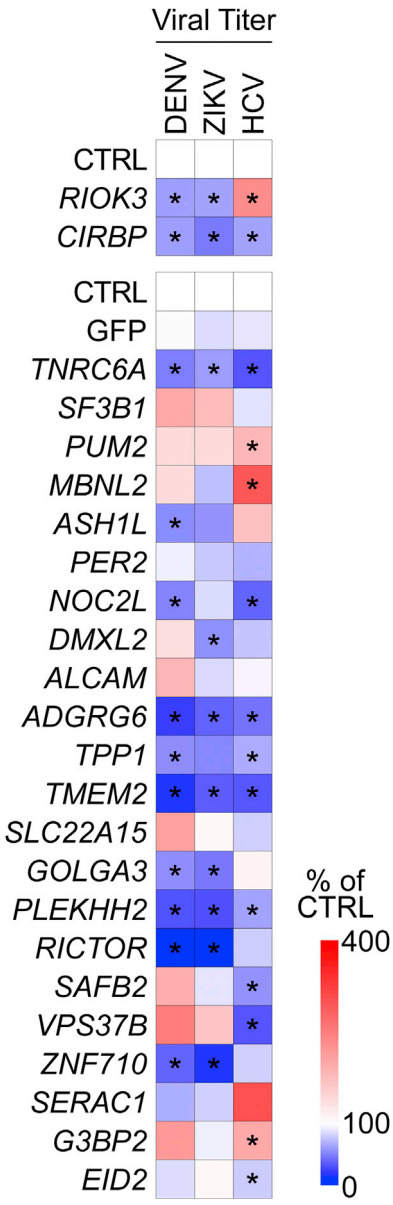

Figure 6. Genes with Infection-Induced m^{6}A Alterations Regulate *Flaviviridae* Infection

Heatmap of viral titers of supernatants harvested from DENV, ZIKV, or HCV-infected cells (48 hpi) treated with the indicated siRNAs. Data are presented as percentage of titer of each virus relative to cells treated with CTRL siRNA. Colors represent the mean of 3 biological replicates. Viral infections were performed at a multiplicity of infection of 0.2. *p < 0.05 by unpaired Student's t test.

See also Figure S6.

after export to the cytoplasm (Ke et al., 2017). At least three processes could modulate the selective m^{6}A modification of specific transcripts during transcription. First, novel interactions of the m^{6}A writers METTL3 and METTL14 with viral-induced or stress-regulated RNA-binding proteins could target these writers to specific mRNAs and lead to m^{6}A changes during infection. For example, RBM15/15B and VIRMA can target the m^{6}A methyltransferase complex to *Xist* long non-coding RNA or to the 3′ UTRs of mRNA, respectively (Patil et al., 2016; Yue et al., 2018). Second, the writers could be recruited to nascent mRNAs by the histone modification H3K36me3, which marks transcriptionally active loci and recruits METTL14 (Huang et al., 2019). Intriguingly, in HepG2 cells, the *CIRBP* locus is marked by H3K36me3, and its transcript contains an m^{6}A peak at the same site that we identified in Huh7 cells (Huang et al., 2019). This suggests that infection- or ER stress-induced depletion of H3K36me3 marks at the *CIRBP* locus could result in reduced m^{6}A of *CIRBP* by METTL3 and METTL14. Third, changes in transcription rates, which have been inversely correlated with m^{6}A deposition in mRNA, could also contribute to m^{6}A modification of specific transcripts during infection (Slobodin et al., 2017). Further, viral infection can affect RNA structure in cellular transcripts; it is possible that altered mRNA structure could result in divergent m^{6}A modification of cellular transcripts during infection (Mizrahi et al., 2018). Perturbing cellular homeostasis by infection therefore has the potential to reveal new insights into the regulation of m^{6}A modification of cellular transcripts.

We hypothesize that during viral infection, m^{6}A regulation of RNA metabolism leads to rapid, tunable changes in mRNA and protein abundance of host factors. While m^{6}A can affect mRNA nuclear export and stability, *Flaviviridae* infection did not affect these processes for either *RIOK3* or *CIRBP* mRNA. Instead, we found that m^{6}A changes promote translation of *RIOK3* and alternative splicing of *CIRBP*. m^{6}A promotes translation of modified mRNAs in multiple contexts by mediating interactions with m^{6}A-binding proteins, including YTHDF1 (Edupuganti et al., 2017; Han et al., 2019; Huang et al., 2018; Li et al., 2017a; Lin et al., 2016; Meyer et al., 2015; Shi et al., 2017, 2018; Wang et al., 2015, 2019). Similarly, the interaction of YTHDF1 with *RIOK3* mRNA during infection promoted RIOK3 translation even in the context of eIF2α phosphorylation and suppression of global translation (Arnaud et al., 2010; Garaigorta and Chisari, 2009; Roth et al., 2017). For *CIRBP*, the loss of m^{6}A following viral infection led to reduced expression of its long isoform. m^{6}A regulates splicing by modulating mRNA interactions with several m^{6}A-binding splicing factors, which suggests that the loss of m^{6}A in *CIRBP* regulates alternative splicing through changes in its interactions with splicing factors (Alarcón et al., 2015; Liu et al., 2015, 2017b; Louloupi et al., 2018; Xiao et al., 2016; Ye et al., 2017; Zhao et al., 2014; Zhou et al., 2019). Interestingly, *CIRBP-L* is not translated as efficiently as *CIRBP-S*; therefore, reducing the relative abundance of the long isoform might be an expeditious mechanism to maintain abundant CIRBP protein levels during cellular stress. How m^{6}A regulates the fate of other mRNAs with altered modification is still unknown, but it is possible that m^{6}A post-transcriptionally affects the abundance of their protein products or splicing isoforms, similar to how it regulates *RIOK3* and *CIRBP*.

RIOK3 promoted DENV and ZIKV infection but inhibited HCV. Interestingly, *RIOK3* can both positively and negatively regulate innate immune responses by either stimulating the interaction between TBK1 and IRF3 or by phosphorylating and inactivating MDA5 (Feng et al., 2014; Shan et al., 2009; Takashima et al., 2015; Willemsen et al., 2017). The differences in the effects of RIOK3 on DENV, ZIKV, and HCV infection could reflect the

different strategies used by these viruses to inhibit host immune responses (Chen et al., 2017; Gack and Diamond, 2016; Gokhale et al., 2014). Further, Willemsen et al. found that while RIOK3 enhanced innate immune activation, it also promoted influenza A virus infection, implying that RIOK3 could have roles in infection beyond innate immunity (Willemsen et al., 2017).

Both CIRBP isoforms were proviral for DENV, ZIKV, and HCV. The biological functions of the individual CIRBP isoforms, which we found have different subcellular localizations, remain unknown. CIRBP can modulate the translation of pro-inflammatory factors and have anti-apoptotic effects in response to various stresses (Liao et al., 2017). During infection, reduction in the long isoform of CIRBP through loss of m^{6}A could inhibit infection, suggesting that this loss of m^{6}A during infection is part of the host response to infection. Alternatively, reduction of the poorly translated long isoform of *CIRBP* mRNA may be a normal part of the cellular stress response to ensure robust production of CIRBP protein, which can then be co-opted by *Flaviviridae* members to facilitate their replication.

Overall, transcripts with altered m^{6}A modification during *Flaviviridae* infection encoded proteins that influenced the outcome of infection. For each virus, approximately half of the factors tested showed either proviral or antiviral effects, while 86% affected the titer of at least one virus. These data suggest that m^{6}A itself does not represent a simple proviral or antiviral mechanism during infection but rather distinctly modulates specific transcripts that ultimately affect the outcome of infection by different members of the *Flaviviridae* family.

The scale of m^{6}A epitranscriptomic changes with virus infection varies greatly among previous reports (Hesser et al., 2018; Lichinchi et al., 2016a; Rubio et al., 2018; Tan et al., 2018; Winkler et al., 2019). Although we identified altered m^{6}A in 58 peaks in 51 transcripts during infection, inherent variance in transcript coverage in MeRIP-seq data means that many replicates are necessary for statistically significant detection of m^{6}A changes (McIntyre et al., 2019). In particular, this means that our analysis (n = 3 per virus) may underestimate the total number of virus-specific, altered m^{6}A peaks. Additionally, we used a more conservative statistical approach than many previous studies to reveal only the most robust peak changes (McIntyre et al., 2019). The changes detected in MeRIP-seq peaks were validated using MeRIP-qRT-PCR; however, these data do not provide the precise ratio of modified to unmodified copies of a transcript or the exact nucleotides that are modified. Biochemical assays like SCARLET or new sequencing methods will be necessary to resolve this question (Liu et al., 2019a; Saletore et al., 2012).

In summary, we found that *Flaviviridae* infection leads to m^{6}A changes in transcripts that can influence viral infection. We identified innate immune activation and the ER stress response as signals that can modulate m^{6}A levels in specific cellular mRNAs. Our work indicates that post-transcriptional regulation of specific transcripts by m^{6}A and other RNA modifications can be an important determinant of the outcome of infection. Indeed, viral infection alters the abundance of several other epitranscriptomic modifications on cellular RNA (McIntyre et al., 2018), revealing that we are only beginning to understand how RNA modifications affect viral infection.

STAR★METHODS

Detailed methods are provided in the online version of this paper and include the following:

- KEY RESOURCES TABLE
- LEAD CONTACT AND MATERIALS AVAILABILITY
- EXPERIMENTAL MODEL AND SUBJECT DETAILS
  - Cell culture
  - Viruses
- METHOD DETAILS
  - MeRIP-seq
  - MeRIP-qRT-PCR
  - qRT-PCR
  - Immunoblotting
  - FLAG-YTHDF RNA immunoprecipitation
  - siRNA treatment and viral infectivity assays
  - Quantification of infection by immunofluorescence
  - Immunofluorescence assay for CIRBP localization
  - Cell fractionation
  - Measurement of RNA stability
  - Polysome profiling
  - *RIOK3* and *CIRBP* cloning and stable cell lines
  - Reporter cloning and luciferase assays
  - ^{35}S pulse-labeled immunoprecipitation
  - LC-MS/MS for m^{6}A/A determination
- QUANTIFICATION AND STATISTICAL ANALYSIS
  - Data analysis for MeRIP-seq and RNA-seq
- DATA AND CODE AVAILABILITY

SUPPLEMENTAL INFORMATION

Supplemental Information can be found online at https://doi.org/10.1016/j.molcel.2019.11.007.

ACKNOWLEDGMENTS

We thank Moonhee Park, Xinhe Yin, Dr. Olga Ilkayeva, Dr. Christopher Nicchitta, and Dr. Heather Vincent for experimental help and advice; colleagues who provided reagents (see STAR Methods); NEB for gift of anti-m^{6}A antibodies; the Metabolomics Core at the Duke Molecular Physiology Institute; the Duke Functional Genomics Core Facility; the Epigenomics Core and the Scientific Computing Unit at Weill Cornell; and Dr. Kate Meyer and Horner lab members for manuscript discussion. This work was supported by funds from Burroughs Wellcome Fund (S.M.H.) and National Institutes of Health: R01AI125416, R21AI129851 (S.M.H. and C.E.M.), 5P30AI064518 (S.M.H.), R01MH117406 (C.E.M.), and R03HL135475 (C.L.H). Other funding sources include: American Heart Association (N.S.G. Pre-doctoral Fellowship, 17PRE33670017), National Science and Engineering Research Council of Canada (A.B.R.M. PGS-D funding), Bert L. and N. Kuggie Vallee Foundation, WorldQuant Foundation, Pershing Square Sohn Cancer Research Alliance, NASA (NNX14AH50G), and startup funds from the UNC Lineberger Comprehensive Cancer Center (H.M.L. and M.D.M).

AUTHOR CONTRIBUTIONS

Conceptualization, N.S.G., A.B.R.M., C.E.M., and S.M.H.; Investigation, N.S.G., A.B.R.M., C.L.H., H.M.L., and M.D.M.; Formal Analysis, A.B.R.M. and N.S.G.; Software, A.B.R.M.; Visualization, N.S.G. and A.B.R.M.; Writing – Original Draft, N.S.G., A.B.R.M., and S.M.H.; Writing – Review and Editing, N.S.G., A.B.R.M., C.L.H., H.M.L., M.D.M., C.E.M., and S.M.H.; Funding Acquisition, N.S.G., A.B.R.M., C.L.H., H.M.L., C.E.M., and S.M.H.

DECLARATION OF INTERESTS

C.E.M. is a cofounder and board member for Biotia and Onegevity Health and an advisor or compensated speaker for Abbvie, Acuamark Diagnostics, ArcBio, Bio-Rad, DNA Genotek, Genialis, Genpro, Illumina, NEB, QIAGEN, Whole Biome, and Zymo Research.

Received: June 18, 2019
Revised: October 11, 2019
Accepted: October 29, 2019
Published: December 3, 2019

REFERENCES

Alarcón, C.R., Goodarzi, H., Lee, H., Liu, X., Tavazoie, S., and Tavazoie, S.F. (2015). HNRNPA2B1 Is a Mediator of m(6)A-Dependent Nuclear RNA Processing Events. Cell *162*, 1299–1308.

Aligeti, M., Roder, A., and Horner, S.M. (2015). Cooperation between the Hepatitis C Virus p7 and NS5B Proteins Enhances Virion Infectivity. J. Virol. *89*, 11523–11533.

Arnaud, N., Dabo, S., Maillard, P., Budkowska, A., Kalliampakou, K.I., Mavromara, P., Garcin, D., Hugon, J., Gatignol, A., Akazawa, D., et al. (2010). Hepatitis C virus controls interferon production through PKR activation. PLoS ONE *5*, e10575.

Barbieri, I., Tzelepis, K., Pandolfini, L., Shi, J., Millán-Zambrano, G., Robson, S.C., Aspris, D., Migliori, V., Bannister, A.J., Han, N., et al. (2017). Promoter-bound METTL3 maintains myeloid leukaemia by m^6A-dependent translation control. Nature *552*, 126–131.

Basanta-Sanchez, M., Temple, S., Ansari, S.A., D'Amico, A., and Agris, P.F. (2016). Attomole quantification and global profile of RNA modifications: Epitranscriptome of human neural stem cells. Nucleic Acids Res. *44*, e26.

Beachboard, D.C., Park, M., Vijayan, M., Snider, D.L., Fernando, D.J., Williams, G.D., Stanley, S., McFadden, M.J., and Horner, S.M. (2019). The small GTPase RAB1B promotes antiviral innate immunity by interacting with TNF receptor-associated factor 3 (TRAF3). J. Biol. Chem. *294*, 14231–14240.

Blázquez, A.B., Escribano-Romero, E., Merino-Ramos, T., Saiz, J.C., and Martín-Acebes, M.A. (2014). Stress responses in flavivirus-infected cells: activation of unfolded protein response and autophagy. Front. Microbiol. *5*, 266.

Bray, N.L., Pimentel, H., Melsted, P., and Pachter, L. (2016). Near-optimal probabilistic RNA-seq quantification. Nat. Biotechnol. *34*, 525–527.

Carletti, T., Zakaria, M.K., Faoro, V., Reale, L., Kazungu, Y., Licastro, D., and Marcello, A. (2019). Viral priming of cell intrinsic innate antiviral signaling by the unfolded protein response. Nat. Commun. *10*, 3889.

Chan, S.W. (2014). Unfolded protein response in hepatitis C virus infection. Front. Microbiol. *5*, 233.

Chen, S., Wu, Z., Wang, M., and Cheng, A. (2017). Innate Immune Evasion Mediated by Flaviviridae Non-Structural Proteins. Viruses *9*, E291.

Conway, J.R., Lex, A., and Gehlenborg, N. (2017). UpSetR: an R package for the visualization of intersecting sets and their properties. Bioinformatics *33*, 2938–2940.

Courtney, D.G., Kennedy, E.M., Dumm, R.E., Bogerd, H.P., Tsai, K., Heaton, N.S., and Cullen, B.R. (2017). Epitranscriptomic Enhancement of Influenza A Virus Gene Expression and Replication. Cell Host Microbe *22*, 377–386.e5.

Cui, X., Zhang, L., Meng, J., Rao, M.K., Chen, Y., and Huang, Y. (2018). MeTDiff: A Novel Differential RNA Methylation Analysis for MeRIP-Seq Data. IEEE/ACM Trans Comput Biol Bioinform *15*, 526–534.

De Maio, F.A., Risso, G., Iglesias, N.G., Shah, P., Pozzi, B., Gebhard, L.G., Mammi, P., Mancini, E., Yanovsky, M.J., Andino, R., et al. (2016). The Dengue Virus NS5 Protein Intrudes in the Cellular Spliceosome and Modulates Splicing. PLoS Pathog. *12*, e1005841.

Diamond, M.S., Shrestha, B., Marri, A., Mahan, D., and Engle, M. (2003). B cells and antibody play critical roles in the immediate defense of disseminated infection by West Nile encephalitis virus. J. Virol. *77*, 2578–2586.

Dobin, A., Davis, C.A., Schlesinger, F., Drenkow, J., Zaleski, C., Jha, S., Batut, P., Chaisson, M., and Gingeras, T.R. (2013). STAR: ultrafast universal RNA-seq aligner. Bioinformatics *29*, 15–21.

Dominissini, D., Moshitch-Moshkovitz, S., Schwartz, S., Salmon-Divon, M., Ungar, L., Osenberg, S., Cesarkas, K., Jacob-Hirsch, J., Amariglio, N., Kupiec, M., et al. (2012). Topology of the human and mouse m6A RNA methylomes revealed by m6A-seq. Nature *485*, 201–206.

Edupuganti, R.R., Geiger, S., Lindeboom, R.G.H., Shi, H., Hsu, P.J., Lu, Z., Wang, S.Y., Baltissen, M.P.A., Jansen, P.W.T.C., Rossa, M., et al. (2017). N^6-methyladenosine (m^6A) recruits and repels proteins to regulate mRNA homeostasis. Nat. Struct. Mol. Biol. *24*, 870–878.

Engel, M., Eggert, C., Kaplick, P.M., Eder, M., Roh, S., Tietze, L., Namendorf, C., Arloth, J., Weber, P., Rex-Haffner, M., et al. (2018). The Role of m(6)A/m-RNA Methylation in Stress Response Regulation. Neuron *99*, 389–403.e9.

Feng, J., De Jesus, P.D., Su, V., Han, S., Gong, D., Wu, N.C., Tian, Y., Li, X., Wu, T.T., Chanda, S.K., and Sun, R. (2014). RIOK3 is an adaptor protein required for IRF3-mediated antiviral type I interferon production. J. Virol. *88*, 7987–7997.

Fink, J., Gu, F., Ling, L., Tolfvenstam, T., Olfat, F., Chin, K.C., Aw, P., George, J., Kuznetsov, V.A., Schreiber, M., et al. (2007). Host gene expression profiling of dengue virus infection in cell lines and patients. PLoS Negl. Trop. Dis. *1*, e86.

Gack, M.U., and Diamond, M.S. (2016). Innate immune escape by Dengue and West Nile viruses. Curr. Opin. Virol. *20*, 119–128.

Garaigorta, U., and Chisari, F.V. (2009). Hepatitis C virus blocks interferon effector function by inducing protein kinase R phosphorylation. Cell Host Microbe *6*, 513–522.

Gilbert, W.V., Bell, T.A., and Schaening, C. (2016). Messenger RNA modifications: Form, distribution, and function. Science *352*, 1408–1412.

Gokhale, N.S., and Horner, S.M. (2017). RNA modifications go viral. PLoS Pathog. *13*, e1006188.

Gokhale, N.S., Vazquez, C., and Horner, S.M. (2014). Hepatitis C Virus. Strategies to Evade Antiviral Responses. Future Virol. *9*, 1061–1075.

Gokhale, N.S., McIntyre, A.B.R., McFadden, M.J., Roder, A.E., Kennedy, E.M., Gandara, J.A., Hopcraft, S.E., Quicke, K.M., Vazquez, C., Willer, J., et al. (2016). N6-Methyladenosine in Flaviviridae Viral RNA Genomes Regulates Infection. Cell Host Microbe *20*, 654–665.

Gonzales-van Horn, S.R., and Sarnow, P. (2017). Making the Mark: The Role of Adenosine Modifications in the Life Cycle of RNA Viruses. Cell Host Microbe *21*, 661–669.

Han, D., Liu, J., Chen, C., Dong, L., Liu, Y., Chang, R., Huang, X., Liu, Y., Wang, J., Dougherty, U., et al. (2019). Anti-tumour immunity controlled through mRNA m^6A methylation and YTHDF1 in dendritic cells. Nature *566*, 270–274.

Hao, H., Hao, S., Chen, H., Chen, Z., Zhang, Y., Wang, J., Wang, H., Zhang, B., Qiu, J., Deng, F., and Guan, W. (2019). N6-methyladenosine modification and METTL3 modulate enterovirus 71 replication. Nucleic Acids Res. *47*, 362–374.

Heinz, S., Benner, C., Spann, N., Bertolino, E., Lin, Y.C., Laslo, P., Cheng, J.X., Murre, C., Singh, H., and Glass, C.K. (2010). Simple combinations of lineage-determining transcription factors prime cis-regulatory elements required for macrophage and B cell identities. Mol. Cell *38*, 576–589.

Hesser, C.R., Karijolich, J., Dominissini, D., He, C., and Glaunsinger, B.A. (2018). N6-methyladenosine modification and the YTHDF2 reader protein play cell type specific roles in lytic viral gene expression during Kaposi's sarcoma-associated herpesvirus infection. PLoS Pathog. *14*, e1006995.

Holbrook, M.R. (2017). Historical Perspectives on Flavivirus Research. Viruses *9*, E97.

Horner, S.M., and Gale, M., Jr. (2013). Regulation of hepatic innate immunity by hepatitis C virus. Nat. Med. *19*, 879–888.

Horner, S.M., Liu, H.M., Park, H.S., Briley, J., and Gale, M., Jr. (2011). Mitochondrial-associated endoplasmic reticulum membranes (MAM) form innate immune synapses and are targeted by hepatitis C virus. Proc. Natl. Acad. Sci. USA *108*, 14590–14595.

Huang, H., Weng, H., Sun, W., Qin, X., Shi, H., Wu, H., Zhao, B.S., Mesquita, A., Liu, C., Yuan, C.L., et al. (2018). Recognition of RNA N^6-methyladenosine by IGF2BP proteins enhances mRNA stability and translation. Nat. Cell Biol. *20*, 285–295.

Huang, H., Weng, H., Zhou, K., Wu, T., Zhao, B.S., Sun, M., Chen, Z., Deng, X., Xiao, G., Auer, F., et al. (2019). Histone H3 trimethylation at lysine 36 guides m^6A RNA modification co-transcriptionally. Nature *567*, 414–419.

Imam, H., Khan, M., Gokhale, N.S., McIntyre, A.B.R., Kim, G.W., Jang, J.Y., Kim, S.J., Mason, C.E., Horner, S.M., and Siddiqui, A. (2018). *N6*-methyladenosine modification of hepatitis B virus RNA differentially regulates the viral life cycle. Proc. Natl. Acad. Sci. USA *115*, 8829–8834.

Ke, S., Pandya-Jones, A., Saito, Y., Fak, J.J., Vågbø, C.B., Geula, S., Hanna, J.H., Black, D.L., Darnell, J.E., Jr., and Darnell, R.B. (2017). m^6A mRNA modifications are deposited in nascent pre-mRNA and are not required for splicing but do specify cytoplasmic turnover. Genes Dev. *31*, 990–1006.

Kennedy, E.M., Whisnant, A.W., Kornepati, A.V., Marshall, J.B., Bogerd, H.P., and Cullen, B.R. (2015). Production of functional small interfering RNAs by an amino-terminal deletion mutant of human Dicer. Proc. Natl. Acad. Sci. USA *112*, E6945–E6954.

Kennedy, E.M., Bogerd, H.P., Kornepati, A.V., Kang, D., Ghoshal, D., Marshall, J.B., Poling, B.C., Tsai, K., Gokhale, N.S., Horner, S.M., and Cullen, B.R. (2016). Posttranscriptional m(6)A Editing of HIV-1 mRNAs Enhances Viral Gene Expression. Cell Host Microbe *19*, 675–685.

Kumar, M., Belcaid, M., and Nerurkar, V.R. (2016). Identification of host genes leading to West Nile virus encephalitis in mice brain using RNA-seq analysis. Sci. Rep. *6*, 26350.

Lee, J.S., Mendez, R., Heng, H.H., Yang, Z.Q., and Zhang, K. (2012). Pharmacological ER stress promotes hepatic lipogenesis and lipid droplet formation. Am. J. Transl. Res. *4*, 102–113.

Li, A., Chen, Y.S., Ping, X.L., Yang, X., Xiao, W., Yang, Y., Sun, H.Y., Zhu, Q., Baidya, P., Wang, X., et al. (2017a). Cytoplasmic m^6A reader YTHDF3 promotes mRNA translation. Cell Res. *27*, 444–447.

Li, Z., Weng, H., Su, R., Weng, X., Zuo, Z., Li, C., Huang, H., Nachtergaele, S., Dong, L., Hu, C., et al. (2017b). FTO Plays an Oncogenic Role in Acute Myeloid Leukemia as a N^6-Methyladenosine RNA Demethylase. Cancer Cell *31*, 127–141.

Liao, Y., Tong, L., Tang, L., and Wu, S. (2017). The role of cold-inducible RNA binding protein in cell stress response. Int. J. Cancer *141*, 2164–2173.

Lichinchi, G., Gao, S., Saletore, Y., Gonzalez, G.M., Bansal, V., Wang, Y., Mason, C.E., and Rana, T.M. (2016a). Dynamics of the human and viral m(6)A RNA methylomes during HIV-1 infection of T cells. Nat. Microbiol. *1*, 16011.

Lichinchi, G., Zhao, B.S., Wu, Y., Lu, Z., Qin, Y., He, C., and Rana, T.M. (2016b). Dynamics of Human and Viral RNA Methylation during Zika Virus Infection. Cell Host Microbe *20*, 666–673.

Lin, S., Choe, J., Du, P., Triboulet, R., and Gregory, R.I. (2016). The m(6)A Methyltransferase METTL3 Promotes Translation in Human Cancer Cells. Mol. Cell *62*, 335–345.

Lindenbach, B.D., Evans, M.J., Syder, A.J., Wölk, B., Tellinghuisen, T.L., Liu, C.C., Maruyama, T., Hynes, R.O., Burton, D.R., McKeating, J.A., and Rice, C.M. (2005). Complete replication of hepatitis C virus in cell culture. Science *309*, 623–626.

Linder, B., Grozhik, A.V., Olarerin-George, A.O., Meydan, C., Mason, C.E., and Jaffrey, S.R. (2015). Single-nucleotide-resolution mapping of m6A and m6Am throughout the transcriptome. Nat. Methods *12*, 767–772.

Liu, N., Dai, Q., Zheng, G., He, C., Parisien, M., and Pan, T. (2015). N(6)-methyladenosine-dependent RNA structural switches regulate RNA-protein interactions. Nature *518*, 560–564.

Liu, L., Zhang, S.W., Huang, Y., and Meng, J. (2017a). QNB: differential RNA methylation analysis for count-based small-sample sequencing data with a quad-negative binomial model. BMC Bioinformatics *18*, 387.

Liu, N., Zhou, K.I., Parisien, M., Dai, Q., Diatchenko, L., and Pan, T. (2017b). N6-methyladenosine alters RNA structure to regulate binding of a low-complexity protein. Nucleic Acids Res. *45*, 6051–6063.

Liu, H., Begik, O., Lucas, M.C., Ramirez, J.M., Mason, C.E., Wiener, D., Schwartz, S., Mattick, J.S., Smith, M.A., and Novoa, E.M. (2019a). Accurate detection of m^6A RNA modifications in native RNA sequences. Nat. Commun. *10*, 4079.

Liu, Y., You, Y., Lu, Z., Yang, J., Li, P., Liu, L., Xu, H., Niu, Y., and Cao, X. (2019b). N^6-methyladenosine RNA modification-mediated cellular metabolism rewiring inhibits viral replication. Science *365*, 1171–1176.

Louloupi, A., Ntini, E., Conrad, T., and Ørom, U.A.V. (2018). Transient N-6-Methyladenosine Transcriptome Sequencing Reveals a Regulatory Role of m6A in Splicing Efficiency. Cell Rep. *23*, 3429–3437.

Love, M.I., Huber, W., and Anders, S. (2014). Moderated estimation of fold change and dispersion for RNA-seq data with DESeq2. Genome Biol. *15*, 550.

Luna, J.M., Scheel, T.K., Danino, T., Shaw, K.S., Mele, A., Fak, J.J., Nishiuchi, E., Takacs, C.N., Catanese, M.T., de Jong, Y.P., et al. (2015). Hepatitis C virus RNA functionally sequesters miR-122. Cell *160*, 1099–1110.

Mauer, J., and Jaffrey, S.R. (2018). FTO, m^6A_m, and the hypothesis of reversible epitranscriptomic mRNA modifications. FEBS Lett. *592*, 2012–2022.

McIntyre, W., Netzband, R., Bonenfant, G., Biegel, J.M., Miller, C., Fuchs, G., Henderson, E., Arra, M., Canki, M., Fabris, D., and Pager, C.T. (2018). Positive-sense RNA viruses reveal the complexity and dynamics of the cellular and viral epitranscriptomes during infection. Nucleic Acids Res. *46*, 5776–5791.

McIntyre, A.B.R., Gokhale, N.S., Cerchietti, L., Jaffrey, S.R., Horner, S.M., and Mason, C.E. (2019). Limits in the detection of m6A changes using MeRIP/m6A-seq. bioRxiv. https://doi.org/10.1101/657130.

Meyer, K.D., and Jaffrey, S.R. (2017). Rethinking m^6A Readers, Writers, and Erasers. Annu. Rev. Cell Dev. Biol. *33*, 319–342.

Meyer, K.D., Saletore, Y., Zumbo, P., Elemento, O., Mason, C.E., and Jaffrey, S.R. (2012). Comprehensive analysis of mRNA methylation reveals enrichment in 3′ UTRs and near stop codons. Cell *149*, 1635–1646.

Meyer, K.D., Patil, D.P., Zhou, J., Zinoviev, A., Skabkin, M.A., Elemento, O., Pestova, T.V., Qian, S.B., and Jaffrey, S.R. (2015). 5′ UTR m(6)A Promotes Cap-Independent Translation. Cell *163*, 999–1010.

Mizrahi, O., Nachshon, A., Shitrit, A., Gelbart, I.A., Dobesova, M., Brenner, S., Kahana, C., and Stern-Ginossar, N. (2018). Virus-Induced Changes in mRNA Secondary Structure Uncover cis-Regulatory Elements that Directly Control Gene Expression. Mol. Cell *72*, 862–874.e5.

Muñoz-Jordán, J.L., and Fredericksen, B.L. (2010). How flaviviruses activate and suppress the interferon response. Viruses *2*, 676–691.

Neufeldt, C.J., Cortese, M., Acosta, E.G., and Bartenschlager, R. (2018). Rewiring cellular networks by members of the Flaviviridae family. Nat. Rev. Microbiol. *16*, 125–142.

Park, S.M., Deering, R.P., Lu, Y., Tivnan, P., Lianoglou, S., Al-Shahrour, F., Ebert, B.L., Hacohen, N., Leslie, C., Daley, G.Q., et al. (2014). Musashi-2 controls cell fate, lineage bias, and TGF-β signaling in HSCs. J. Exp. Med. *211*, 71–87.

Patil, D.P., Chen, C.K., Pickering, B.F., Chow, A., Jackson, C., Guttman, M., and Jaffrey, S.R. (2016). m(6)A RNA methylation promotes XIST-mediated transcriptional repression. Nature *537*, 369–373.

Query, C.C., and Keene, J.D. (1987). A human autoimmune protein associated with U1 RNA contains a region of homology that is cross-reactive with retroviral p30gag antigen. Cell *51*, 211–220.

Quicke, K.M., Bowen, J.R., Johnson, E.L., McDonald, C.E., Ma, H., O'Neal, J.T., Rajakumar, A., Wrammert, J., Rimawi, B.H., Pulendran, B., et al. (2016). Zika Virus Infects Human Placental Macrophages. Cell Host Microbe *20*, 83–90.

Reimand, J., Arak, T., Adler, P., Kolberg, L., Reisberg, S., Peterson, H., and Vilo, J. (2016). g:Profiler-a web server for functional interpretation of gene lists (2016 update). Nucleic Acids Res. *44* (W1), W83-9.

Robinson, M.D., McCarthy, D.J., and Smyth, G.K. (2010). edgeR: a Bioconductor package for differential expression analysis of digital gene expression data. Bioinformatics *26*, 139–140.

Rosenberg, B.R., Depla, M., Freije, C.A., Gaucher, D., Mazouz, S., Boisvert, M., Bédard, N., Bruneau, J., Rice, C.M., and Shoukry, N.H. (2018). Longitudinal transcriptomic characterization of the immune response to acute hepatitis C virus infection in patients with spontaneous viral clearance. PLoS Pathog. *14*, e1007290.

Roth, H., Magg, V., Uch, F., Mutz, P., Klein, P., Haneke, K., Lohmann, V., Bartenschlager, R., Fackler, O.T., Locker, N., et al. (2017). Flavivirus Infection Uncouples Translation Suppression from Cellular Stress Responses. MBio *8*, e02150–16.

Rubio, R.M., Depledge, D.P., Bianco, C., Thompson, L., and Mohr, I. (2018). RNA m^6 A modification enzymes shape innate responses to DNA by regulating interferon β. Genes Dev. *32*, 1472–1484.

Saito, T., Owen, D.M., Jiang, F., Marcotrigiano, J., and Gale, M., Jr. (2008). Innate immunity induced by composition-dependent RIG-I recognition of hepatitis C virus RNA. Nature *454*, 523–527.

Saletore, Y., Meyer, K., Korlach, J., Vilfan, I.D., Jaffrey, S., and Mason, C.E. (2012). The birth of the Epitranscriptome: deciphering the function of RNA modifications. Genome Biol. *13*, 175.

Schindelin, J., Arganda-Carreras, I., Frise, E., Kaynig, V., Longair, M., Pietzsch, T., Preibisch, S., Rueden, C., Saalfeld, S., Schmid, B., et al. (2012). Fiji: an open-source platform for biological-image analysis. Nat. Methods *9*, 676–682.

Schwartz, S., Mumbach, M.R., Jovanovic, M., Wang, T., Maciag, K., Bushkin, G.G., Mertins, P., Ter-Ovanesyan, D., Habib, N., Cacchiarelli, D., et al. (2014). Perturbation of m6A writers reveals two distinct classes of mRNA methylation at internal and 5′ sites. Cell Rep. *8*, 284–296.

Schwerk, J., Jarret, A.P., Joslyn, R.C., and Savan, R. (2015). Landscape of post-transcriptional gene regulation during hepatitis C virus infection. Curr. Opin. Virol. *12*, 75–84.

Sergushichev, A.A. (2016). An algorithm for fast preranked gene set enrichment analysis using cumulative statistic calculation. bioRxiv. https://doi.org/10.1101/060012.

Sessions, O.M., Barrows, N.J., Souza-Neto, J.A., Robinson, T.J., Hershey, C.L., Rodgers, M.A., Ramirez, J.L., Dimopoulos, G., Yang, P.L., Pearson, J.L., and Garcia-Blanco, M.A. (2009). Discovery of insect and human dengue virus host factors. Nature *458*, 1047–1050.

Sessions, O.M., Tan, Y., Goh, K.C., Liu, Y., Tan, P., Rozen, S., and Ooi, E.E. (2013). Host cell transcriptome profile during wild-type and attenuated dengue virus infection. PLoS Negl. Trop. Dis. *7*, e2107.

Shan, J., Wang, P., Zhou, J., Wu, D., Shi, H., and Huo, K. (2009). RIOK3 interacts with caspase-10 and negatively regulates the NF-kappaB signaling pathway. Mol. Cell. Biochem. *332*, 113–120.

Shi, H., Wang, X., Lu, Z., Zhao, B.S., Ma, H., Hsu, P.J., Liu, C., and He, C. (2017). YTHDF3 facilitates translation and decay of N^6-methyladenosine-modified RNA. Cell Res. *27*, 315–328.

Shi, H., Zhang, X., Weng, Y.L., Lu, Z., Liu, Y., Lu, Z., Li, J., Hao, P., Zhang, Y., Zhang, F., et al. (2018). m^6A facilitates hippocampus-dependent learning and memory through YTHDF1. Nature *563*, 249–253.

Shi, H., Wei, J., and He, C. (2019). Where, When, and How: Context-Dependent Functions of RNA Methylation Writers, Readers, and Erasers. Mol. Cell *74*, 640–650.

Slobodin, B., Han, R., Calderone, V., Vrielink, J., Loayza-Puch, F., Elkon, R., and Agami, R. (2017). Transcription Impacts the Efficiency of mRNA Translation via Co-transcriptional N6-adenosine Methylation. Cell *169*, 326–337.e12.

Stern-Ginossar, N., Thompson, S.R., Mathews, M.B., and Mohr, I. (2019). Translational Control in Virus-Infected Cells. Cold Spring Harb. Perspect. Biol. *11*, a033001.

Su, A.I., Pezacki, J.P., Wodicka, L., Brideau, A.D., Supekova, L., Thimme, R., Wieland, S., Bukh, J., Purcell, R.H., Schultz, P.G., and Chisari, F.V. (2002). Genomic analysis of the host response to hepatitis C virus infection. Proc. Natl. Acad. Sci. USA *99*, 15669–15674.

Sumpter, R., Jr., Loo, Y.M., Foy, E., Li, K., Yoneyama, M., Fujita, T., Lemon, S.M., and Gale, M., Jr. (2005). Regulating intracellular antiviral defense and permissiveness to hepatitis C virus RNA replication through a cellular RNA helicase, RIG-I. J. Virol. *79*, 2689–2699.

Supek, F., Bošnjak, M., Škunca, N., and Šmuc, T. (2011). REVIGO summarizes and visualizes long lists of gene ontology terms. PLoS ONE *6*, e21800.

Suthar, M.S., Aguirre, S., and Fernandez-Sesma, A. (2013). Innate immune sensing of flaviviruses. PLoS Pathog. *9*, e1003541.

Takashima, K., Oshiumi, H., Takaki, H., Matsumoto, M., and Seya, T. (2015). RIOK3-mediated phosphorylation of MDA5 interferes with its assembly and attenuates the innate immune response. Cell Rep. *11*, 192–200.

Tan, B., Liu, H., Zhang, S., da Silva, S.R., Zhang, L., Meng, J., Cui, X., Yuan, H., Sorel, O., Zhang, S.W., et al. (2018). Viral and cellular N^6-methyladenosine and N^6,2′-O-dimethyladenosine epitranscriptomes in the KSHV life cycle. Nat. Microbiol. *3*, 108–120.

Thrift, A.P., El-Serag, H.B., and Kanwal, F. (2017). Global epidemiology and burden of HCV infection and HCV-related disease. Nat. Rev. Gastroenterol. Hepatol. *14*, 122–132.

Tirumuru, N., Zhao, B.S., Lu, W., Lu, Z., He, C., and Wu, L. (2016). N(6)-methyladenosine of HIV-1 RNA regulates viral infection and HIV-1 Gag protein expression. eLife *5*, e15528.

Tsai, K., Courtney, D.G., and Cullen, B.R. (2018). Addition of m6A to SV40 late mRNAs enhances viral structural gene expression and replication. PLoS Pathog. *14*, e1006919.

Vaquero-Garcia, J., Barrera, A., Gazzara, M.R., González-Vallinas, J., Lahens, N.F., Hogenesch, J.B., Lynch, K.W., and Barash, Y. (2016). A new view of transcriptome complexity and regulation through the lens of local splicing variations. eLife *5*, e11752.

Vazquez, C., Tan, C.Y., and Horner, S.M. (2019). Hepatitis C virus infection is inhibited by a non-canonical antiviral signaling pathway targeted by NS3-NS4A. J Virol. *93*, e00725–19.

Vu, L.P., Pickering, B.F., Cheng, Y., Zaccara, S., Nguyen, D., Minuesa, G., Chou, T., Chow, A., Saletore, Y., MacKay, M., et al. (2017). The N^6-methyladenosine (m^6A)-forming enzyme METTL3 controls myeloid differentiation of normal hematopoietic and leukemia cells. Nat. Med. *23*, 1369–1376.

Wang, X., Zhao, B.S., Roundtree, I.A., Lu, Z., Han, D., Ma, H., Weng, X., Chen, K., Shi, H., and He, C. (2015). N(6)-methyladenosine Modulates Messenger RNA Translation Efficiency. Cell *161*, 1388–1399.

Wang, H., Hu, X., Huang, M., Liu, J., Gu, Y., Ma, L., Zhou, Q., and Cao, X. (2019). Mettl3-mediated mRNA m^6A methylation promotes dendritic cell activation. Nat. Commun. *10*, 1898.

Wek, R.C. (2018). Role of eIF2α Kinases in Translational Control and Adaptation to Cellular Stress. Cold Spring Harb. Perspect. Biol. *10*, a032870.

Willemsen, J., Wicht, O., Wolanski, J.C., Baur, N., Bastian, S., Haas, D.A., Matula, P., Knapp, B., Meyniel-Schicklin, L., Wang, C., et al. (2017). Phosphorylation-Dependent Feedback Inhibition of RIG-I by DAPK1 Identified by Kinome-wide siRNA Screening. Mol. Cell *65*, 403–415.e8.

Williams, G.D., Gokhale, N.S., and Horner, S.M. (2019). Regulation of Viral Infection by the RNA Modification N6-Methyladenosine. Annu. Rev. Virol. *6*, 235–253.

Winkler, R., Gillis, E., Lasman, L., Safra, M., Geula, S., Soyris, C., Nachshon, A., Tai-Schmiedel, J., Friedman, N., Le-Trilling, V.T.K., et al. (2019). m^6A modification controls the innate immune response to infection by targeting type I interferons. Nat. Immunol. *20*, 173–182.

Xiao, W., Adhikari, S., Dahal, U., Chen, Y.S., Hao, Y.J., Sun, B.F., Sun, H.Y., Li, A., Ping, X.L., Lai, W.Y., et al. (2016). Nuclear m(6)A Reader YTHDC1 Regulates mRNA Splicing. Mol. Cell *61*, 507–519.

Yang, Y., Hsu, P.J., Chen, Y.S., and Yang, Y.G. (2018). Dynamic transcriptomic m^6A decoration: writers, erasers, readers and functions in RNA metabolism. Cell Res. *28*, 616–624.

Ye, F., Chen, E.R., and Nilsen, T.W. (2017). Kaposi's Sarcoma-Associated Herpesvirus Utilizes and Manipulates RNA N(6)-Adenosine Methylation To Promote Lytic Replication. J. Virol. *91*, e00466–17.

Yue, Y., Liu, J., Cui, X., Cao, J., Luo, G., Zhang, Z., Cheng, T., Gao, M., Shu, X., Ma, H., et al. (2018). VIRMA mediates preferential m^6A mRNA methylation in 3'UTR and near stop codon and associates with alternative polyadenylation. Cell Discov. *4*, 10.

Zanini, F., Pu, S.Y., Bekerman, E., Einav, S., and Quake, S.R. (2018). Single-cell transcriptional dynamics of flavivirus infection. eLife *7*, e32942.

Zhang, Y., Liu, T., Meyer, C.A., Eeckhoute, J., Johnson, D.S., Bernstein, B.E., Nusbaum, C., Myers, R.M., Brown, M., Li, W., and Liu, X.S. (2008). Model-based analysis of ChIP-Seq (MACS). Genome Biol. *9*, R137.

Zhao, X., Yang, Y., Sun, B.F., Shi, Y., Yang, X., Xiao, W., Hao, Y.J., Ping, X.L., Chen, Y.S., Wang, W.J., et al. (2014). FTO-dependent demethylation of N6-methyladenosine regulates mRNA splicing and is required for adipogenesis. Cell Res. *24*, 1403–1419.

Zhong, X., Yu, J., Frazier, K., Weng, X., Li, Y., Cham, C.M., Dolan, K., Zhu, X., Hubert, N., Tao, Y., et al. (2018). Circadian Clock Regulation of Hepatic Lipid Metabolism by Modulation of m(6)A mRNA Methylation. Cell Rep. *25*, 1816–1828.e4.

Zhou, J., Wan, J., Shu, X.E., Mao, Y., Liu, X.M., Yuan, X., Zhang, X., Hess, M.E., Bruning, J.C., and Qian, S.B. (2018). N(6)-Methyladenosine Guides mRNA Alternative Translation during Integrated Stress Response. Mol. Cell *69*, 636–647.e7.

Zhou, K.I., Shi, H., Lyu, R., Wylder, A.C., Matuszek, Z., Pan, J.N., He, C., Parisien, M., and Pan, T. (2019). Regulation of Co-transcriptional Pre-mRNA Splicing by m(6)A through the Low-Complexity Protein hnRNPG. Mol. Cell *76*, 70–81.e9.

STAR★METHODS

KEY RESOURCES TABLE

REAGENT or RESOURCE	SOURCE	IDENTIFIER
Antibodies		
Anti-METTL3	Novus Biologicals	Cat# H00056339-B01P; RRID:AB_2687437
Anti-METTL14	Sigma-Aldrich	Cat# HPA038002; RRID:AB_10672401
Anti-WTAP	Proteintech	Cat# 60188-1-Ig; RRID:AB_10859484
Anti-FTO	Abcam	Cat# ab92821; RRID:AB_10565042
Anti-ALKBH5	Sigma-Aldrich	Cat# HPA007196; RRID:AB_1850461
Anti-YTHDF1	Proteintech	Cat# 17479-1-AP; RRID:AB_2217473
Anti-YTHDF2	Proteintech	Cat# 24744-1-AP; RRID:AB_2687435
Anti-YTHDF3	Sigma-Aldrich	Cat# SAB2102736; RRID:AB_10599885
Anti-FLAG	Sigma-Aldrich	Cat# F7425; RRID:AB_439687
Anti-FLAG-HRP conjugated	Sigma-Aldrich	Cat# A8592; RRID:AB_439702
Anti-Tubulin	Sigma-Aldrich	Cat# T5168; RRID:AB_477579
Anti-DENV NS3	GeneTex	Cat# GT2811; RRID:AB_2538763
Anti-ZIKV NS3	GeneTex	Cat# GTX133320
Anti-HCV NS4A	Genscript custom antibody (Horner et al., 2011)	N/A
Anti-DENV/ZIKV E (4G2)	Made in lab from hybridoma	ATCC Cat# HB-112; RRID:CVCL_J890
Anti-HCV NS5A	9E10, gift from Dr. Charles Rice (Lindenbach et al., 2005)	N/A
Anti-RIOK3	Proteintech	Cat# 13593-1-AP; RRID:AB_2178105
Anti-CIRBP	Proteintech	Cat# 10209-2-AP; RRID:AB_2080263
Anti-eIF2α	Cell Signaling Tech.	Cat# 9722; RRID:AB_2230924
Anti-Phospho-eIF2α	Cell Signaling Tech.	Cat# 3398; RRID:AB_2096481
Anti-HSPA5	Cell Signaling Tech.	Cat# 3177; RRID:AB_2119845
Anti-GADD34	Proteintech	Cat# 10449-1-AP; RRID:AB_2168724
Anti-H2A.X	Cell Signaling Tech.	Cat# 9718; RRID:AB_2118009
Anti-U170K serum	Gift of Dr. Jack Keene (Query and Keene, 1987)	N/A
Normal rabbit IgG	Cell Signaling Tech.	Cat# 2729; RRID:AB_1031062
Anti-mouse HRP Secondary	Jackson ImmunoResearch	Cat# 115-035-003; RRID:AB_10015289
Anti-rabbit HRP Secondary	Jackson ImmunoResearch	Cat# 111-035-003; RRID:AB_2313567
Anti-mouse IRDye 800	LI-COR Biosciences	Cat# 926-32212; RRID:AB_621847
Anti-rabbit IRDye 800	LI-COR Biosciences	Cat# 926-32211; RRID:AB_621843
Anti-mouse AlexaFluor 488	Thermo Fisher Sci.	Cat# A11001; RRID:AB_2534069
Bacterial and Virus Strains		
Dengue virus (DENV; New Guinea C)	Sessions et al., 2009	N/A
Zika virus (ZIKV, Puerto Rico 2015, PRVABC59)	Quicke et al., 2016	N/A
West Nile virus (WNV; New York-2000)	Diamond et al., 2003	N/A
Hepatitis C virus (HCV; JFH-1 strain, culture adapted)	Aligeti et al., 2015	N/A
Chemicals, Peptides, and Recombinant Proteins		
Thapsigargin	Tocris	Cat# 1138; CAS: 67526-95-8
N6-methyladenosine 5′ monophosphate salt	Santa Cruz Biotech.	Cat# sc-215524; CAS: 81921-35-9
Human IFN-β	PBL Assay Science	Cat# 11415-1
TRIzol	Thermo Fisher Sci.	Cat# 15596026

(*Continued on next page*)

Continued

REAGENT or RESOURCE	SOURCE	IDENTIFIER
TRIzol LS	Thermo Fisher Sci.	Cat# 10296010
NP-40	Thermo Fisher Sci.	Cat# 85124
n-Dodecyl-β-D-maltoside (DDM)	Chem-Impex	Cat# 21950
Puromycin	Sigma-Aldrich	Cat# P8833
Cycloheximide	Sigma-Aldrich	Cat# 7698
Blasticidin	Thermo Fisher Sci.	Cat# R21001
Recombinant RNaseIN RNase inhibitor	Promega	Cat# N2511
Protease inhibitor	Sigma-Aldrich	Cat# P8340
Phosphatase inhibitor	Thermo Fisher Sci.	Cat# 78426
NotI-HF	New England Biolabs	Cat# R3189
PmeI	New England Biolabs	Cat# R0560
XhoI	New England Biolabs	Cat# R0146
NruI-HF	New England Biolabs	Cat# R3192
BamHI-HF	New England Biolabs	Cat# R3136
BglII	New England Biolabs	Cat# R0144
Hoescht 33342	Thermo Fisher Sci.	Cat# 62249
Actinomycin D	Sigma-Aldrich	Cat# A9415
2X Laemmli sample buffer	Bio-Rad	Cat# 161-0737
Nuclease P1	Sigma-Aldrich	Cat# N8630
Antarctic phosphatase	New England Biolabs	Cat# M0289
Protein G Dynabeads	Thermo Fisher Sci.	Cat# 10004D
FLAG M2 conjugated beads	Sigma-Aldrich	Cat# M8823; RRID: RRID:AB_2637089
^{35}S	PerkinElmer	Cat# NEG772007MC
Opti-MEM I reduced serum medium	Thermo Fisher Sci.	Cat# 31985070
Methionine/cysteine-free DMEM	Sigma-Aldrich	Cat# D0422
Critical Commercial Assays		
N6-methyladenosine enrichment kit	New England Biolabs	Cat# E1610S
Dynabeads mRNA purification kit	Thermo Fisher Sci.	Cat# 61006
NEBNext rRNA depletion kit	New England Biolabs	Cat# E6310S
Power SYBR Green PCR master mix	Thermo Fisher Sci.	Cat# 4367659
Dual luciferase reporter assay system	Promega	Cat# E1960
CellTiter-Glo luminescent cell viability assay	Promega	Cat# G7571
Protein assay dye-reagent concentrate	Bio-Rad	Cat# 5000006
iScript cDNA synthesis kit	Bio-Rad	Cat# 1708891BUN
Superscript III enzyme	Thermo Fisher Sci.	Cat# 18080044
InFusion HD cloning kit	Takara Bio	Cat# 639650
Quik-change Lightning SDM kit	Agilent	Cat# 210518
RNA fragmentation reagent	Thermo Fisher Sci	Cat# AM8740
Trans-IT mRNA transfection reagent	Mirus	Cat# MIR2225
FuGENE 6 transfection reagent	Promega	Cat# E2691
Lipofectamine RNAiMAX transfection reagent	Thermo Fisher Sci.	Cat# 13778150
CloneAmp HiFi PCR premix	Clontech	Cat# 639298
VIP peroxidase substrate kit	Vector Laboratories	Cat# SK-4600
TURBO DNase	Thermo Fisher Sci	Cat# AM2239
Deposited Data		
MeRIP-seq of mRNA from DENV, ZIKV, WNV, and HCV infected (MOI 1, 48 h) and uninfected Huh7 cells	This study	GEO: GSE130891

(*Continued on next page*)

Continued

REAGENT or RESOURCE	SOURCE	IDENTIFIER
MeRIP-seq of mRNA from HCV PAMP treated (8 h), TG treated (16 h) and untreated Huh7 cells	This study	GEO: pending
Experimental Models: Cell Lines		
Huh7	Gift of Dr. Michael Gale, Jr. (Sumpter et al., 2005)	RRID: RRID:CVCL_0336
Huh7.5	Gift of Dr. Michael Gale, Jr. (Sumpter et al., 2005)	RRID: RRID:CVCL_7927
293T	ATCC	ATCC Cat# CRL-3216; RRID:CVCL_0063
Vero	ATCC	ATCC Cat# CCL-81; RRID:CVCL_0059
C6/36	ATCC	ATCC Cat# CRL-1660; RRID:CVCL_Z230
Huh7 IRF3 KO	Vazquez et al., 2019	N/A
Huh7 FLAG-GFP	Gokhale et al., 2016	N/A
Huh7 FLAG-YTHDF1	Gokhale et al., 2016	N/A
Huh7 FLAG-RIOK3-1	This study	N/A
Huh7 FLAG-RIOK3-2	This study	N/A
Huh7 FLAG-CIRBP-S-1	This study	N/A
Huh7 FLAG-CIRBP-S-2	This study	N/A
Huh7 FLAG-CIRBP-L-1	This study	N/A
Huh7 FLAG-CIRBP-L-2	This study	N/A
Huh7 m^6A-null RLuc – RIOK3 3′UTR WT	This study	N/A
Huh7 m^6A-null RLuc – RIOK3 3′UTR m^6A-mut	This study	N/A
Oligonucleotides		
Oligonucleotides for qRT-PCR	Table S4	N/A
Oligonucleotides and gBocks for Cloning	Table S4	N/A
Oligonucleotides for siRNA	Table S4	N/A
Recombinant DNA		
pLEX-RIOK3	This study	N/A
pLEX-CIRBP-S	This study	N/A
pLEX-CIRBP-L	This study	N/A
psiCheck2 m^6A-null RIOK3-3′UTR WT	This study	N/A
psiCheck2 m^6A-null RIOK3-3′UTR m^6A-mut	This study	N/A
psiCheck2 m^6A-null RLuc-CIRBP-splicing WT	This study	N/A
psiCheck2 m^6A-null RLuc-CIRBP-splicing m^6A-mut	This study	N/A
pcDNA-Blast	Kennedy et al., 2015	N/A
psPAX2	Duke Functional Genomics Core Facility	Addgene plasmid # 12260; RRID:Addgene_12260
pMD2.G	Duke Functional Genomics Core Facility	Addgene Plasmid #12259; RRID:Addgene_12259
Software and Algorithms		
ImageStudio	LI-COR Biosciences	RRID:SCR_013715; https://www.licor.com/bio/products/software/image_studio_lite
Fiji	Schindelin et al., 2012	RRID:SCR_002285 https://fiji.sc
Prism 8.0	Graphpad	RRID:SCR_002798; https://www.graphpad.com
STAR	Dobin et al., 2013	v2.5.0a, https://github.com/alexdobin/STAR
MACS2	Zhang et al., 2008	v2.1.1.20160309, https://github.com/taoliu/MACS
DESeq2	Love et al., 2014	v1.20.0, https://bioconductor.org/packages/release/bioc/html/DESeq2.html

(*Continued on next page*)

Continued

REAGENT or RESOURCE	SOURCE	IDENTIFIER
edgeR	Robinson et al., 2010	v3.22.3, https://bioconductor.org/packages/release/bioc/html/edgeR.html
QNB	Liu et al., 2017a	v1.1.11, https://cran.r-project.org/src/contrib/Archive/QNB/
CovFuzze	Imam et al., 2018	v0.1.3, https://github.com/al-mcintyre/CovFuzze
gProfiler	Reimand et al., 2016	ve95_eg42_p13_f6e58b9, https://biit.cs.ut.ee/gprofiler/gost
REVIGO	Supek et al., 2011	http://revigo.irb.hr/
HOMER	Heinz et al., 2010	v4.9.1, http://homer.ucsd.edu/homer/motif/
fgsea	Sergushichev, 2016	v1.8.0, https://bioconductor.org/packages/release/bioc/html/fgsea.html
UpSetR	Conway et al., 2017	v1.3.3, https://CRAN.R-project.org/package=UpSetR

LEAD CONTACT AND MATERIALS AVAILABILITY

Further information and requests for resources and reagents should be directed to and will be fulfilled by the Lead Contact, Stacy M. Horner (stacy.horner@duke.edu).

EXPERIMENTAL MODEL AND SUBJECT DETAILS

Cell culture

Huh7 and Huh-7.5 cells (gift of Dr. Michael Gale Jr., University of Washington (Sumpter et al., 2005)), Huh7 IRF3 KO cells (Vazquez et al., 2019), 293T cells (ATCC: CRL-3216) Vero cells (ATCC: CCL-81), C6/36 (ATCC: CRL-1660) were grown in Dulbecco's modification of Eagle's medium (DMEM; Mediatech) supplemented with 10% fetal bovine serum (HyClone), 25 mM HEPES (Thermo Fisher), and 1X non-essential amino acids (Thermo Fisher), referred to as complete DMEM (cDMEM). Huh7 and Huh-7.5 cells were verified using the Promega GenePrint STR kit (DNA Analysis Facility, Duke University), and cells were verified as mycoplasma free by the LookOut Mycoplasma PCR detection kit (Sigma-Aldrich).

Viruses

Infectious stocks of a cell culture-adapted strain of genotype 2A JFH1 HCV were generated and titered in Huh-7.5 cells by focus-forming assay (FFA), as described (Aligeti et al., 2015). DENV2-NGC (Sessions et al., 2009), ZIKV-PR2015 (Quicke et al., 2016), and WNV-NY2000 (Diamond et al., 2003) stocks were prepared in C6/36 insect cells and titered in Vero cells, as described. For viral infections, cells were incubated in a low volume of cDMEM containing virus at a multiplicity of infection (MOI) of 1 for 2-3 h (except when otherwise stated), following which cDMEM was replenished. Cells were infected for 48 h unless otherwise described. To quantify virus, cellular supernatants were analyzed by FFA.

METHOD DETAILS

MeRIP-seq

Huh7 cells seeded in 15 cm plates were infected with DENV, ZIKV, WNV, or HCV (MOI 1) or left uninfected (mock-infected). At 48 h post-infection, total RNA was extracted using TRIzol (Thermo Fisher) and treated with TURBO DNase I (Thermo Fisher). mRNA was purified from 200 μg total RNA from each sample using the Dynabeads mRNA purification kit (Thermo Fisher) and concentrated by ethanol precipitation. mRNA was fragmented using the RNA Fragmentation Reagent (Thermo Fisher) for 15 min and purified by ethanol precipitation. MeRIP was performed using EpiMark *N6*-methyladenosine Enrichment kit (NEB) according to the manufacturer's recommendations with the following modifications. Briefly, 25 μL Protein G Dynabeads (Thermo Fisher) per sample were washed three times in MeRIP buffer (150 mM NaCl, 10 mM Tris-HCl [pH 7.5], 0.1% NP-40), and incubated with 1 μL anti-m^6A antibody for 2 h at 4°C with rotation. After washing three times with MeRIP buffer, anti-m^6A conjugated beads were incubated with purified mRNA with rotation at 4°C overnight in 300 μL MeRIP buffer with 1 μL RNase inhibitor (recombinant RNasin; Promega). 10% of the mRNA sample was saved as the input fraction. Beads were then washed twice with 500 μL MeRIP buffer, twice with low salt wash buffer (50 mM NaCl, 10 mM Tris-HCl [pH 7.5], 0.1% NP-40), twice with high salt wash buffer (500 mM NaCl, 10 mM Tris-HCl [pH 7.5], 0.1% NP-40), and once again with MeRIP buffer. m^6A-modified RNA was eluted twice in 100 μL of MeRIP buffer containing 5 mM m^6A salt (Santa Cruz Biotechnology) for 30 min at 4°C with rotation. Eluates were pooled and concentrated by ethanol purification.

RNA-seq libraries were prepared from both eluate and 10% input mRNA using the TruSeq mRNA library prep kit (Illumina), subjected to quality control (MultiQC), and sequenced on the HiSeq 4000 instrument.

MeRIP-qRT-PCR

For MeRIP-qRT-PCR, total RNA was harvested from uninfected and infected Huh7 and Huh7 IRF3 KO cells seeded in 10 cm plates or 6-well plates at 48 h post-infection. For ER-stress induction, cells seeded in 6-well plates were treated with 500 nM thapsigargin (Tocris) for 16 h. For interferon treatment, cells seeded in 6-well plates were incubated with 100 U/mL human IFN-β (PBL Assay Science) for 24 h. HCV PAMP was prepared by *in vitro* transcription, as described (Beachboard et al., 2019; Saito et al., 2008). 2.5 μg of HCV PAMP RNA was transfected into cells seeded in 6-well plates for 8 h using the Mirus mRNA transfection kit. At the indicated time points for each experiment, RNA was extracted and MeRIP-qRT-PCR was performed like MeRIP-seq with some differences. Specifically, total RNA was prepared from cells using TRIzol, and diluted to equivalent concentrations. Then, 20-50 μg total RNA was fragmented for 3 min, purified by ethanol precipitation, and resuspended in 30 μL water. 0.1 fmol of positive control (m^6A-modified *Gaussia* luciferase RNA) and negative control (unmodified *Cypridina* luciferase RNA) spike-ins supplied with the EpiMark *N6*-methyladenosine Enrichment kit were added to each sample. Following MeRIP as described above, eluates were concentrated by ethanol precipitation. 1 μL input and the entire IP fractions were reverse transcribed using the iScript cDNA synthesis kit (BioRad) and subjected to qRT-PCR. Primer sequences are supplied in Table S4. Relative m^6A level for each transcript was calculated as the percent of input in each condition normalized to that of the respective positive control spike-in. Fold change of enrichment was calculated with mock samples normalized to 1.

qRT-PCR

The iScript cDNA synthesis kit (Bio-Rad) was used for reverse transcription of total RNA samples. qRT-PCR was performed using the Applied Biosystems QuantStudio 6 Flex real-time PCR instrument. To measure relative abundance of *CIRBP* isoforms, total RNA was reverse transcribed with the Superscript III enzyme (Invitrogen) using a gene specific primer. qRT-PCR was performed using specific primers that detect *CIRBP* isoforms. The expression of each isoform was normalized to invariant region of *CIRBP*. Primer sequences are provided in Table S4.

Immunoblotting

Cell lysates were prepared in a modified RIPA buffer (10 mM Tris [pH 7.5], 150 mM NaCl, 0.5% sodium deoxycholate, and 1% Triton X-100) supplemented with protease inhibitor cocktail (Sigma-Aldrich) and phosphatase inhibitor cocktail II (Millipore), and clarified by centrifugation. Protein concentration was determined by Bradford assay (Bio-Rad). 5-15 μg of protein was resolved by SDS/PAGE and transferred to nitrocellulose membranes using the Trans-Blot Turbo System (Bio-Rad). Membranes were blocked in 5% milk in phosphate buffered saline with 0.1% Tween (PBS-T) and incubated with the relevant primary antibodies. After washing three times with PBS-T, membranes were incubated with species-specific horseradish peroxidase-conjugated antibodies (Jackson ImmunoResearch, 1:5000) or fluorescent antibodies (LI-COR, IRDye 800, 1:5000). Chemiluminescence (Clarity ECL, Bio-Rad) or fluorescence was detected on a LI-COR Odyssey Fc instrument and analyzed using the ImageStudio software. The following antibodies were used for immunoblot: anti-METTL3 (Novus Biologicals, 1:1000), anti-METTL14 (Sigma-Aldrich, 1:5000), anti-FTO (Abcam, 1:1000), anti-YTHDF1 (Proteintech, 1:1000), anti-YTHDF2 (Proteintech, 1:1000), anti-YTHDF3 (Sigma-Aldrich, 1:1000), anti-ALKBH5 (Sigma-Aldrich, 1:1000), anti-WTAP (Proteintech, 1:1000) anti-FLAG M2 (Sigma-Aldrich, 1:5000), anti-tubulin (Sigma-Aldrich, 1:5000), anti-HCV NS5A (clone 9E10, gift of Charles Rice, Rockefeller University (Lindenbach et al., 2005), 1:1000), anti-RIOK3 (Proteintech, 1:1000), anti-CIRBP (Proteintech 1:1000), anti-DENV NS3 (GeneTex, 1:1000), anti-ZIKV NS3 (GeneTex, 1:1000), anti-HCV NS4A (Genscript custom (Horner et al., 2011)), 1:1000), anti-eIF2α (Cell Signaling, 1:1000), anti-phospho-eIF2α (Cell Signaling, 1:1000), anti-GADD34 (Proteintech, 1:1000), anti-HSPA5 (Cell Signaling, 1:1000), anti-H2A.X (Cell Signaling, 1:1000), anti-U170K serum (gift of Dr. Jack Keene, Duke University, (Query and Keene, 1987), 1:1000).

FLAG-YTHDF RNA immunoprecipitation

Generation of Huh7 cells stably expressing FLAG-GFP or FLAG-YTHDF1 was described previously (Gokhale et al., 2016). Cells seeded in 6-well plates were infected with DENV, ZIKV, or HCV (MOI 1). At 48 h post-infection cells were harvested by trypsinization and lysed in polysome lysis buffer (100 mM KCl, 5 mM $MgCl_2$, 10 mM HEPES [pH 7.0], 0.5% NP-40), supplemented with protease inhibitor cocktail (Sigma-Aldrich) and RNase inhibitor (RNasin), and cleared by centrifugation. Protein was quantified by Bradford assay, and 200 μg ribonucleoprotein complexes were immunoprecipitated with M2 anti-FLAG conjugated magnetic beads (Sigma-Aldrich) overnight at 4°C with rotation in NT2 buffer (50 mM Tris-HCl [pH 7.5], 150 mM NaCl, 1 mM $MgCl_2$, 0.05% NP-40). Beads were washed five times in ice-cold NT2 buffer. Protein for immunoblotting was eluted from ten percent of beads by boiling in 2X Laemmli sample buffer (Bio-Rad). RNA was extracted from ninety percent of beads using TRIzol reagent (Thermo Fisher). Equal volumes of eluted RNA were used for cDNA synthesis, quantified by qRT-PCR, and normalized to RNA levels in input samples. Fold enrichment was calculated with FLAG-GFP and mock samples set as 1.

siRNA treatment and viral infectivity assays

Cells seeded in 24-well plates were transfected with siRNA against intended targets (QIAGEN, sequences provided in Table S4) using Lipofectamine RNAiMAX (Thermo Fisher) according to the manufacturer's recommendation. At 24 h post-transfection, cells were infected with DENV, ZIKV, and HCV (MOI 0.2). At 48 (targeted siRNA screen) or 72 (RIOK3 and CIRBP depletion) h post-infection, virus titer in the supernatant was measured by FFA. Serial dilutions of supernatants were used to infect naive Vero (DENV and ZIKV) or Huh-7.5 (HCV) cells in triplicate wells of a 48-well plate. At 72 h post-infection, cells were fixed in cold 1:1 methanol:acetone and immunostained with 4G2 antibody purified in the lab from a hybridoma (for DENV and ZIKV, 1:2000), or anti-HCV NS5A (1:2000). Following binding of horseradish peroxidase conjugated secondary antibody (1:1000; Jackson ImmunoResearch), infected foci were visualized with the VIP Peroxidase Substrate Kit (Vector Laboratories) and counted at 40X magnification. Titer was calculated using the following formula: (dilution factor x number of foci x 1000) / volume of infection (μl), resulting in units of focus forming units / mL (FFU/mL). Depletion of siRNA targets was confirmed by qRT-PCR (primer sequences in Table S4). Cellular viability after siRNA treatment was measured by the Cell-Titer Glo assay (Promega) according to the manufacturer's recommendation.

For testing the effect of YTHDF1 on RIOK3 translation, cells plated in 6-well plates were transfected with siRNAs against YTHDF1 (QIAGEN, Table S4) at 24 and 48 h following seeding. 24 h after the second round of transfection, cells were infected DENV, and lysates were harvested at 48 h post-transfection and subjected to immunoblotting.

Quantification of infection by immunofluorescence

To measure percent of cells infected following viral infection, Huh7 cells seeded in 96-well plates were infected with DENV, ZIKV, WNV, or HCV (MOI 1). Cells were fixed in cold 1:1 methanol:acetone at the indicated h post-infection, and immunostained with 4G2 antibody (DENV, ZIKV, WNV) or anti-HCV NS5A. Following binding of AlexaFluor 488-conjugated secondary antibody (Thermo Fisher) and nuclear staining with Hoechst (Thermo Fisher), cells were imaged using the Cellomics Arrayscan VTI robotic microscope at the Duke Functional Genomics Core Facility. The percentage of infected cells was determined by measuring cells stained for viral antigen relative to the total number of nuclei.

Immunofluorescence assay for CIRBP localization

Huh7 cells stably expressing FLAG-tagged CIRBP-S and CIRBP-L were plated in 4-well chamber slides (Millipore) and infected with the indicated virus (MOI 1). At 48 h post-infection, cells were fixed in 4% paraformaldehyde, permeabilized with 0.2% Triton X-100 (Sigma-Aldrich), and immunostained with anti-FLAG (Sigma-Aldrich, 1:1000) antibody, or antibody against viral antigens (4G2 for DENV and ZIKV (1:1000); anti-NS5A (1:1000) for HCV). Following treatment with AlexaFluor dye-conjugated secondary antibodies (Thermo Fisher) and the nuclear stain Hoescht, coverslips were mounted with ProLong Gold (Thermo Fisher) and imaged on a Leica DM4 B fluorescence microscope using a 63X objective. Images were processed with the Fiji software (Schindelin et al., 2012).

Cell fractionation

Fractionation of cells to isolate chromatin-associated RNA was performed as described (Ke et al., 2017). Briefly, cells were collected from 10 cm plates by trypsinization, lysed in 200 μL cytoplasmic lysis buffer (10 mM Tris-HCL [pH 7.4], 150 mM NaCl, 0.15% NP-40) on ice for 5 min, and passed through 500 μl 24% sucrose cushion by centrifugation at 12000 xG for 10 min at 4°C. The supernatant (cytoplasmic fraction) was then removed and the nuclear pellet was rinsed twice with cold phosphate buffered saline (PBS). The nuclear pellet was resuspended in 100 μL ice cold glycerol buffer (20 mM Tris-HCL [pH 7.4], 75 mM NaCl, 0.5 mM EDTA, 1 mM DTT, 125 μM PMSF, 50% glycerol). 100 μL nuclear lysis buffer (10 mM HEPES [pH 7.4], 1 mM DTT, 7.5 mM $MgCl_2$, 0.2 mM EDTA, 300 mM NaCl, 1 M urea, 1% NP-40) was added to the suspension, followed by brief vortexing, and incubation on ice for 2 min. Samples were centrifuged for 2 min at 4°C at 12000 xG and the supernatant (nuclear fraction) was removed. The chromatin pellet was rinsed twice with cold PBS, resuspended in 50 μL DNase I buffer with 2 U Turbo DNase I (Invitrogen), and incubated at 37°C for 30 min. RNA was then extracted from the chromatin fraction using TRIzol reagent and subjected to MeRIP-qRT-PCR. The cytoplasmic, nuclear, and chromatin fractions were subjected to immunoblotting to analyze fractionation.

For nuclear/cytoplasmic fractionation to investigate mRNA export, uninfected and infected (MOI 1) cells grown in 10 cm plates were harvested by trypsinization and lysed in 200 μL lysis buffer (10mM Tris-HCl [pH 7.4], 140 mM NaCl, 1.5 mM $MgCl_2$, 10 mM EDTA, 0.5% NP-40) on ice for 5 min. Following centrifugation at 12000 xG at 4°C for 5 min, the supernatant (cytoplasmic fraction) was collected, and the nuclear pellet was rinsed twice with lysis buffer. RNA was extracted from cytoplasmic and nuclear pellets using TRIzol reagent and analyzed by qRT-PCR.

Measurement of RNA stability

Cells plated in 24-well plates were infected with the indicated virus (MOI 1). At 36 h post-infection, media was changed to cDMEM containing 1 μM Actinomycin D (Sigma-Aldrich). RNA was extracted from cells at the indicated time points post-treatment using TRIzol reagent and analyzed by qRT-PCR. Data were normalized as the percent of RNA remaining at each time point after treatment, relative to that at the time of treatment.

Polysome profiling

Mock- and DENV-infected (MOI 1) Huh7 cells plated in 10 cm plates were harvested by trypsinization at 48 h post infection following a 10 min pulse with cycloheximide (0.2 mM; Sigma-Aldrich) and were lysed in cytoplasmic lysis buffer (200 mM KCl, 25 mM HEPES pH 7.0, 10 mM $MgCl_2$, 2% n-Dodecyl β-D-maltoside (DDM; Chem-Impex), 0.2 mM cycloheximide (Sigma-Aldrich), 1 mM DTT, 40 U RNaseIn) for 15 min on ice. Following clarification, lysates were ultracentrifuged on 15%–50% sucrose gradients prepared in polysome gradient buffer (200 mM KCl, 25 mM HEPES pH 7.0, 15 mM $MgCl_2$, 1 mM DTT, 0.2 mM cycloheximide) at 35,000 xG for 3.5 h at 4°C. Following ultracentrifugation, 16 fractions were collected from each sample using a BioComp Piston Gradient Fractionator instrument fitted with a TRIAX flow cell to measure absorbance. RNA was extracted from each fraction using TRIzol LS reagent (Thermo Fisher), and RNA quality was checked on a 1% agarose gel. Following cDNA synthesis using the iScript cDNA synthesis kit, qRT-PCR was performed using primers specific for the long and short isoforms of *CIRBP*.

RIOK3 and *CIRBP* cloning and stable cell lines

All primer sequences used for cloning are provided in Table S4. *RIOK3* (GenBank: NM_003831.4), as well as both long (GenBank: NM_001300829) and short (GenBank: NM_001280) isoforms of *CIRBP,* were cloned by PCR (HiFi PCR premix, Clontech) from cDNA from Huh7 cells prepared with the Superscript III RT kit (Thermo Fisher) using the oligo$(dT)_{20}$ primer. PCR products were inserted into pLEX-FLAG lentiviral vector between the *NotI* and *XhoI* sites using the InFusion HD cloning kit (Takara Bio) to generate constructs with N-terminal FLAG tags. Lentivirus was produced from 293T cells transfected with pLEX vectors and packaging plasmids psPAX2 and pMD2.G (provided by Duke Functional Genomics Facility). Huh7 cells were transduced by these lentiviruses and stable cell lines expressing FLAG-RIOK3, FLAG-CIRBP-S, and FLAG-CIRBP-L were selected using puromycin (2 μg/mL; Sigma-Aldrich). Single cell clones were obtained by serial dilution and verified by immunoblotting. Cell lines were maintained in cDMEM containing 1 μg/mL puromycin.

Reporter cloning and luciferase assays

All primer and gBlock sequences are provided in Table S4. To generate m^6A null *RIOK3* reporters, the *Renilla* and Firefly luciferase genes in psiCheck2 plasmid (Promega) were first replaced by constructs with synonymous mutations in putative m^6A sites (obtained as IDT gBlocks). The wild type *RIOK3* 3′ UTR was cloned from Huh7 cDNA (GenBank: NM_003831.4) and inserted after the m^6A null *Renilla* luciferase gene in the multiple cloning site of psiCheck2 between *XhoI* and *NotI* using the InFusion HD kit. m^6A-mut *RIOK3* 3′ UTR (in which all putative m^6A sites were mutated from A to T) was obtained as a gBlock and also inserted between these restriction sites. WT and m^6A-mut *RIOK3* reporter plasmids along with the pcDNA-Blast plasmid (Kennedy et al., 2015) were linearized using BamHI and BglII respectively, purified by ethanol precipitation and co-transfected into Huh7 cells in 6-well plates (90 ng reporter, 10 ng pcDNA-Blast) using FuGENE 6 transfection reagent (Promega). Cells were selected with blasticidin (0.2 μg/mL; Thermo Fisher) and single cell clones stably expressing WT and m^6A-mut reporters were isolated. For MeRIP-qRT-PCR of reporter RNA, WT and m^6A-mut expressing cells were plated in 6-well plates, infected with the indicated virus (MOI 1), and RNA was extracted using TRIzol at 48 h post-infection. Following MeRIP as described, qRT-PCR was performed to discriminate reporter RNA using a forward primer within the *Renilla* luciferase gene and a reverse primer in the *RIOK3* 3′ UTR. For luciferase assays, WT and m^6A-mut expressing cells in 24-well plates were infected with the indicated virus (MOI 1) and dual luciferase assay (Promega) was performed at 48 h post-infection according to the manufacturer's instructions. Data was normalized as the value of Renilla luminescence divided by Firefly luminescence, and values for mock-infected cells were set as 1.

To generate *CIRBP* splicing reporters, *CIRBP* exon 5 – 3′ UTR (Hg38;chr19:127553-1273172) was amplified by PCR from genomic DNA. A fragment of m^6A null *Renilla* luciferase beyond the *NruI* site and up to the stop codon was amplified by PCR with overlapping ends with *Renilla* luciferase (5′; before the *NruI* site) and the *CIRBP* fragment (3′). These fragments were inserted into *NruI-XhoI* digested psiCheck2 m^6A null plasmid using the InFusion HD kit. m^6A-mut *CIRBP* reporter was generated by mutating the essential C in the m^6A site synonymously to T using two rounds of site-directed mutagenesis with the QuikChange Lightning kit (Agilent).

^{35}S pulse-labeled immunoprecipitation

Huh7 cells seeded in 10 cm plates were infected with DENV (MOI 1) or left uninfected. At 45 h post-infection, media was removed and 3 mL warm methionine/cysteine-free DMEM was added to plates. After 15 min of incubation, 3 mL methionine/cysteine-free DMEM containing 100 mCi ^{35}S (Perkin Elmer) was added. Cells were harvested at 3 h post-treatment and lysed in RIPA buffer. 300 μg protein was incubated with 4 μg anti-RIOK3 antibody (Proteintech) or normal rabbit IgG (Cell Signaling) in 300 μL RIPA buffer overnight at 4°C with rotation. Antibody-protein complexes were then incubated with 40 μL pre-washed protein G Dynabeads (Thermo Fisher) for 2 h. Protein was eluted from beads in 2X Laemmli buffer. Eluates were resolved by SDS/PAGE. Gels were fixed in solution containing 50% methanol and 10% acetic acid, dried, and subjected to autoradiography on film.

LC-MS/MS for m^6A/A determination

mRNA was purified from 200 μg total RNA extracted from uninfected and infected Huh7 cells (MOI 1, 48 h post-infection) using one round of polyA selection (Dynabeads mRNA purification kit; Thermo Fisher) and one round of rRNA depletion (NEBNext rRNA depletion kit, NEB). After ethanol precipitation, purified mRNA was digested into mononucleotides with nuclease P1 (Sigma-Aldrich, 2 U) in buffer containing 25 mM NaCl and 2.5 mM $ZnCl_2$ for 2 h at 37°C, followed by incubation with Antarctic Phosphatase (NEB, 5 U) for an

additional 2 h at 37°C. Nucleosides were separated and quantified using UPLC-MS/MS as previously described, except acetic acid was used in place of formic acid (Basanta-Sanchez et al., 2016).

QUANTIFICATION AND STATISTICAL ANALYSIS

Western blot images were acquired and analyzed using Li-Cor Image Studio. Microscopy pictures were processed in Fiji. Figure panels were processed and organized using Adobe Illustrator CC. qRT-PCR and MeRIP-qRT-PCR data was analyzed using Microsoft Excel. Graphpad Prism 8 was used to generate graphs, to determine the mean, standard deviation or standard error, and to perform statistical analyses, as described in the figure legends.

Data analysis for MeRIP-seq and RNA-seq

Reads were aligned using STAR (Dobin et al., 2013) to the human reference genome (hg38), combined with the appropriate virus genome for each infected sample. Differential gene expression between infected and uninfected samples was compared using DESeq2 (Love et al., 2014). UpSet plots of the intersects between genes regulated with individual viruses were generated using UpSetR (Conway et al., 2017). Gene ontology for RNA-seq changes in Figure S1D was analyzed using gProfiler, with redundant GO terms collapsed using REVIGO (Reimand et al., 2016; Supek et al., 2011). For gProfiler, upregulated genes with $Log_2FC \geq 2$ and adjusted p value < 0.05 with all viruses were considered. There were very few consistently downregulated genes at $Log_2FC \leq -2$ (particularly for ZIKV), so we expanded our set to genes with smaller $Log_2FC \leq -0.5$, downregulated by DENV, HCV, and WNV infection. For REVIGO, we allowed similarity of up to 0.5, with semantic similarity calculated using SimRel. Adjusted p values were provided for the REVIGO calculations. Gene set enrichment analyses using fgsea in R showed similar differentially regulated pathways as gProfiler (Sergushichev, 2016). "Infection-annotated" genes and peaks were summarized for Figure 1B based on gene inclusion in "Infectious disease," "Unfolded Protein Response (UPR)," "Interferon Signaling," and "Innate Immune System" Reactome pathways from fgsea.

We called m^6A peaks from MeRIP-seq using MACS2 (Zhang et al., 2008) and used all peaks detected in at least two replicates for further analysis. Motif enrichment was calculated using HOMER for Figure 1C (Heinz et al., 2010). Metagene plots for methylated DRACH motifs were plotted using a custom script. DRACH motifs were considered methylated if detected under m^6A peaks in at least 2 biological replicates. Relative positions of m^6A peaks within genes are based on the transcripts with the highest mean coverage per gene, as calculated with kallisto (Bray et al., 2016).

We identified m^6A peaks changes using a generalized linear model (adapted from (Park et al., 2014)), and the QNB program (Liu et al., 2017a). In brief (see Park et al., 2014 or McIntyre et al., 2019 for more details), a generalized linear model following the equation

$$\log\mu_{ij} = \beta_{0i} + \beta_{IPi}X_{IPj} + \beta_{VIRi}X_{VIRj} + \beta_{IP:VIRi}X_{IP:VIRj} + \log N_j$$

was fit with the following parameters for each peak i and sample j: $X_{IP} = 1$ for immunoprecipitated samples and 0 for input samples, and $X_{VIR} = 1$ for infected samples and 0 for mock. A library size parameter was included for normalization (N) with edgeR (Robinson et al., 2010). The full model was compared to a reduced model without the infection:IP interaction term using a likelihood ratio test of the difference between deviances, implemented through DESeq2 (Love et al., 2014) or edgeR. To control for changes in gene expression, changes in gene expression were subtracted from changes in IP peak reads for significantly modified peaks from DESeq2, edgeR, and QNB, with a threshold for absolute difference in Log_2 fold change of ≥ 1. Significant peaks were further filtered for location within exons, DRACH motif content, and mean input read counts of ≥ 10 to produce the final set of 58 peak changes.

Peaks of interest were plotted for visual evaluation using CovFuzze (https://github.com/al-mcintyre/CovFuzze) (Imam et al., 2018).

DATA AND CODE AVAILABILITY

The raw data from MeRIP-seq analysis of uninfected, HCV PAMP, TG-treated, and infected Huh7 cells have been deposited and are available through GEO: GSE130891 and GEO: GSE138730.